LOAN COPY: RETURN TO
AFSWC (SWOIL)
KIRTLAND AFB, NMEX

NASA
TN
D-1269
C. 1

NASA TN D-1269

TECH LIBRARY KAFB, NM
0153701

TECHNICAL NOTE

D-1269

IMPACT CHARACTERISTICS OF VARIOUS MATERIALS OBTAINED BY AN ACCELERATION-TIME-HISTORY TECHNIQUE APPLICABLE TO EVALUATING REMOTE TARGETS

By John Locke McCarty and Huey D. Carden

Langley Research Center
Langley Station, Hampton, Va.

NATIONAL AERONAUTICS AND SPACE ADMINISTRATION
WASHINGTON June 1962

TECH LIBRARY KAFB, NM
0153701

TABLE OF CONTENTS

	Page
SUMMARY	1
INTRODUCTION	2
SYMBOLS	3
APPARATUS AND TEST PROCEDURE	4
Low-Velocity Impact (5 to 30 fps)	4
Description of projectiles and targets	4
Instrumentation	5
Test procedure	5
High-Velocity Impact (190 to 900 fps)	5
Description of projectiles and targets	5
Description of air gun	6
Instrumentation	6
Test procedure	7
PRESENTATION AND DISCUSSION OF RESULTS	8
General Discussion	8
Application of Available Theories	10
Elastic impacts	10
Plastic impacts	11
Penetration impacts	14
Low-Velocity Impact (5 to 30 fps)	14
Concrete	14
Lead	16
Balsa	17
Sod	19
Sand	20
High-Velocity Impact (190 to 900 fps)	21
Application of Results	22
CONCLUSIONS	24
REFERENCES	26
FIGURES	28

NATIONAL AERONAUTICS AND SPACE ADMINISTRATION

TECHNICAL NOTE D-1269

IMPACT CHARACTERISTICS OF VARIOUS MATERIALS OBTAINED BY AN ACCELERATION-TIME-HISTORY TECHNIQUE APPLICABLE TO EVALUATING REMOTE TARGETS

By John Locke McCarty and Huey D. Carden

SUMMARY

The impact characteristics of several metallic projectiles on a variety of target materials were examined over a range of impact variables by means of a technique applicable to the evaluation of the physical properties of remote surfaces such as the moon. Studies were made of acceleration time histories recorded during the impact process and measurements taken of significant crater dimensions.

Acceleration time histories were obtained at velocities up to 30 fps during the impact of projectiles of various size and mass on concrete, lead, balsa, sod, and sand targets and at velocities up to 225 fps during the impact of 3-inch-diameter projectiles, having different mass and nose shapes, on soil targets. The characteristics evaluated from the acceleration time histories included the pulse shape, the magnitude of the peak acceleration, the time required to reach that acceleration, and the total duration of the pulse. The results indicate that useful information on the hardness or penetrability of any target material may be obtained if a measure of either the peak acceleration during the impact or the corresponding total pulse time is known. It appears from a comparison of the magnitude of these characteristics resulting from impact in all target materials that a relative resistance to penetration, or hardness, scale can be established. From such a scale, the surface hardness of a remote target, such as the moon, may be described in terms of the hardness of accessible earth materials by comparing the acceleration time histories measured during impact of projectiles on the lunar surface with those of identical projectiles during the impacts on known earth materials.

The data for the various impact characteristics are presented as a function of either the impact velocity or parameters composed of variables contained in available impact theories or developed from empirical analyses of the experimental findings.

INTRODUCTION

During the past half-century considerable effort has been devoted to the study of various aspects of impact phenomena. Impact studies have been conducted in the field of ordnance and ballistics, in machine-shop operations, and in many other areas where impulsive forces are involved. Research in these areas, however, has been confined to the immediate needs of the particular program. For example, in ordnance and ballistics, measurements have been made by numerous investigators (refs. 1 and 2, for example) of the penetration depths of projectiles, bombs, and missiles into a variety of targets to evaluate the corresponding impact damage mechanisms.

L
1
6
7
0

Advent of vehicles capable of interplanetary travel has posed interesting new impact problems requiring additional research in the field. One such problem is that of evaluating the cratering and damage resulting from the possible impact of very high-velocity meteoric particles with space vehicles. Considerable research has been devoted to the examination of this particular impact problem and publications discussing the results are available. For example, references 3, 4, and 5 have included results on the high-speed impact (up to 20,000 fps in some cases) of small projectiles in metal targets and reference 6 has extended the investigations to include nonmetallic targets. The results of these tests have been reported primarily in the form of measured dimensions of the crater resulting from the impact.

Another new problem associated with space travel is the achievement of successful landings of vehicles on celestial targets, specifically the moon. A successful landing of an intact payload on the lunar surface requires that the generated landing loads not exceed the structural capabilities of the vehicle and that the vehicle remain on the surface in a tenable position. Both of these requirements necessitate a knowledge of certain basic physical properties of the surface material which are reflected in its resistance to penetration. However, such data pertaining to the lunar surface are presently unknown and, as such, lunar-landing studies to date (for example, ref. 7), must be based upon a material having assumed surface characteristics.

This report discusses the results of an investigation of the relatively low-velocity-impact characteristics of projectiles on various media to obtain possible relationships between such characteristics and certain physical properties of the target material and to provide a background of basic information for use in the design of lunar-landing structures. This investigation utilized a technique which is capable of evaluating similar impact characteristics of remote surfaces, such as the moon. The technique consisted of studying acceleration time

histories recorded during the impact process and, in addition, measuring significant crater characteristics.

SYMBOLS

a	acceleration, in./sec^2 unless otherwise indicated
D	diameter of projectiles, in.
D_c	diameter of blast crater, in. (see fig. 28)
E	modulus of elasticity, lb/sq in.
F	applied load or resisting force, lb
m	mass of projectile, lb-sec^2/in.
p	dynamic flow pressure, lb/sq in.
r	radius of crater at target surface, in.
t	arbitrary time, sec
t_r	rise time for peak acceleration in acceleration time history, sec
t_t	total time for acceleration time history, sec
V_i	impact velocity of projectile, in./sec unless otherwise indicated
V_r	restitution velocity of projectile, in./sec
y	penetration depth of projectile into target measured from target surface to projectile nose, in.
α	maximum relative compression of bodies in collision, in.
$\delta = \frac{1 - \mu^2}{E\pi}$	sq in./lb
μ	Poisson's ratio
k	constant

Subscripts:

A	initial peak acceleration in multiple peak acceleration time history
B	second peak acceleration in multiple peak acceleration time history
max	maximum
p	projectile
t	target

L
1
6
7
0

APPARATUS AND TEST PROCEDURE

Impact studies were conducted over two ranges of test velocity: 5 to 30 fps (low-velocity impacts) and 190 to 900 fps (high-velocity impacts). The apparatus and test procedures employed in these two ranges of velocity differed, primarily because of the dictates of the test requirements. Whereas the low-velocity-impact tests permitted the use of the gravity drop principle to obtain the desired impact velocities, the high-velocity tests necessitated the use of a mechanism to propel the projectile to the desired velocities. Most of the low-velocity tests were performed in the laboratory under readily controlled conditions and permitted the use of a variety of projectiles, whereas the high-velocity tests required field operations and the use of projectiles with sufficient strength to withstand both the propelling and penetrating forces. Photographs and sketches of the various projectiles, component parts, and testing apparatus are presented in figures 1 to 4.

Low-Velocity Impact (5 to 30 fps)

Description of projectiles and targets.- The projectiles used in the low-velocity-impact tests consisted of five configurations constructed of cold rolled steel with hemispherical noses tempered to approximately 42 on the Rockwell C scale. A photograph of these configurations is given in figure 1 together with a tabulation of the mass and diameter of each configuration. Projectiles having diameters of 1, 2, and 3 inches were studied at identical masses; however, the 2-inch-diameter projectile was equipped to receive additional weights so that configurations could be studied at three mass values: 0.0025, 0.0104, and 0.0204 lb-sec^2/in.

Targets for the low-velocity-impact tests included deep concrete, cast lead, balsa with a density of 7.1 lb/cu ft, sod with a high

percentage of sand and having an approximate surface density of 115 lb/cu ft, and dry No. 000 sand. The concrete, lead, sod, and sand materials were selected in an effort to provide targets in each of the categories of impact types discussed in a subsequent section of the present paper. Balsa was selected as a target material because it has application in the impact field as an energy absorber. The balsa target was alined so that the longitudinal axis of the projectile, upon impact, was perpendicular to the target grain. The target thickness in all cases was at least four times as great as the maximum measured penetration in that target.

Instrumentation.- Each projectile was equipped with a crystal accelerometer which was oriented along the longitudinal axis of the projectile to sense the accelerations incurred during the impact process. (See fig. 1(a).) Signals from the accelerometer were routed through a cathode follower and a low pass filter system (cut-off frequency of 5 kc) to a memoscope where they were recorded as a voltage-time trace on a calibrated display screen. Photographs were taken of the accelerometer traces on the display screen following impact, representative samples of which are reproduced in figure 5 where the voltage has been converted to acceleration in g units.

Test procedure.- The testing technique involved impacting each of the five projectiles into the five target materials at velocities of 5, 10, 15, 20, and 30 fps and recording the measured impact characteristics. The desired velocity was obtained by means of the gravity-drop principle wherein the projectile was released at a height above the target corresponding to the desired velocity. Each test was performed at least three times. The impact characteristics measured during and following the tests included the acceleration time histories and, whenever possible, the resulting penetration depths and crater dimensions.

High-Velocity Impact (190 to 900 fps)

Description of projectiles and targets.- The projectiles used in the high-velocity-impact studies were designed to withstand not only the impact forces but also the forces necessary to propel the projectile to the desired impact velocity. The basic configuration consisted of a tempered steel casing, 3 inches in diameter and 8 inches long, which had thin copper plating on the external surfaces to avoid possible damage to the propelling mechanism. A photograph of such a projectile is presented in figure 2 which also shows the various components that are either mounted within or screwed to the projectile. The accelerometers are mounted within a 2.3-inch-diameter hole which extended $6\frac{1}{2}$ inches into the base of the projectile. The projectile cap, which receives the notched release bolt, is screwed into the base of the projectile. Projectiles having both hemispherical nose shapes, as shown in figure 2,

and conical nose shapes with a 60° included angle were examined during these high-velocity tests. Variations in the projectile mass, from approximately 0.023 to 0.045 lb-sec^2/in. were achieved by rigidly attaching additional masses to the base of the projectile.

In general, the target for these high-velocity-impact tests was the local soil which had approximately the following characteristics: a sod surface having a density of about 115 lb/cu ft beneath which extended a 1-foot layer of silty sand, a 3-foot layer of sandy clay, a 3-foot layer of clay sand followed by a considerable depth of silty sand containing frequent shells. The water table extended to within approximately 5 feet of the surface. Several additional tests were conducted with lighter projectiles made of aluminum impacting less dense materials such as peat moss and dry portland cement.

L
1
6
7
0

Description of air gun.- The air gun pictured in figure 3 and shown schematically in figure 4 was used to propel the projectiles to the desired impact velocities. The basic element of this gun is a 6-inch-diameter pipe 20.55 feet in length. The upper end of the pipe serves as a pressure chamber and a 3-inch-diameter, 11.25-foot-long, smooth bore barrel is installed in the lower or muzzle end. With the gun in firing position, the barrel is held in place by means of the flange at the lower end of the gun and the projectile, sealed by "O" rings, is located in the barrel just below the transition section. The projectile, equipped with a notched release bolt, is held in place, prior to firing, by the support rod which extends the entire length of the pressure chamber as shown in the sketch of figure 4. The operation of the gun is simply one of bleeding compressed air into the pressure chamber until the force on the rear of the projectile exceeds the ultimate strength of the release bolt which has been notched to fail at a desired loading.

The gun is mounted on a tripod as shown in figure 3 and is equipped with lifting lugs to permit the use of hoists for lowering it to a loading position. In the initial steps of the reloading process, the breech block is removed from the gun casing and the support rod, with the remains of the release bolt still attached, is extracted completely from the pressure chamber. A projectile, together with a new release bolt, is then screwed to the support rod and, after the necessary electrical connections, is inserted into the pressure chamber and seated in the barrel. The breech block is then bolted to the gun casing and the complete assembly raised into position for firing.

Instrumentation.- The projectiles of the high-velocity-impact tests were equipped with two accelerometers to sense the accelerations incurred during the impact process. These accelerometers (shown in fig. 2) were rigidly mounted within the projectile and oriented along the longitudinal axis. Acceleration time histories of the impacts were obtained from the crystal accelerometer, shown in the figure mounted on a counterbalance which was installed to oppose the weight of the copper-ball accelerometer.

The accelerometer signals were routed within the gun through a nylon-protected low-noise-level coaxial cable which extended from the accelerometer to a high-pressure fitting in the breech block. From the breech block the signals were routed through protected shielded cable to first a cathode follower and then to the memoscope where they were recorded as voltage-time traces on the calibrated display screen. Samples of such recorded traces are presented in figures 5(g) and 5(h) where the voltage has been converted to acceleration in g units.

In addition to the crystal accelerometer which depended upon trouble-free circuitry for success, each of the projectiles was equipped with a copper-ball accelerometer. Copper-ball accelerometers are one of a variety of peak reading, unidirectional, self-contained, mechanical gages which, because of their compactness and simplicity, have been used extensively for shock measurements. The principle of their operation (discussed fully in ref. 8) is one of deforming a copper ball when an acceleration is applied to the accelerometer housing. The permanent plastic deformation of the ball is then measured with micrometers and the peak acceleration is deduced from a static calibration curve of the copper ball.

The projectile velocity was measured by means of an electronic counter which recorded the time required for the projectile to complete two electrical circuits separated a known distance along the projectile path prior to impact. Each of the two electrical circuits consisted of a pair of wires mounted to a framework below the air gun muzzle as shown in figure 4. The electronic counter was triggered by the projectile as it completed the circuit in the first pair of wires and stopped when the projectile completed the circuit in the second pair of wires.

Test procedure.- The testing technique involved impacting the test projectiles into local soil at velocities up to 900 fps by means of the air gun and recording the associated impact characteristics. The projectile velocity was controlled by the dimensions of the notch in the release bolt which was designed to fail at a chamber pressure necessary to propel the projectile at a desired velocity. The operation of the air gun is explained in the section entitled "Description of air gun."

Acceleration time histories recorded on the memoscope were successfully obtained during impacts from the crystal accelerometers at projectile velocities up to 225 fps. Difficulties with this trailing-wire technique precluded the use of crystal accelerometers at higher velocities. Measurements of peak accelerations by the copper-ball accelerometer, however, were obtained at all impact velocities. In addition to the acceleration characteristics, measurements were made of the penetration depths of the impacting projectiles.

PRESENTATION AND DISCUSSION OF RESULTS

General Discussion

An analysis of the acceleration time histories (or "signatures") recorded during the impact of the test projectiles on various targets together with measurements of the resulting craters permitted the evaluation of the impact characteristics of the various projectile-target combinations. Reproduced samples of acceleration time histories recorded during the impact of intact projectiles on the various nondestructive target materials investigated in both the low- and high-velocity studies are presented in figure 5. These histories constitute the variation of acceleration of the projectile with time throughout the impact process. The figures show that the impact of the test projectile on different target materials produces acceleration time histories that differ significantly according to the impact type. In general, the impact of a projectile on a target may be classified as a combination of one or more of three basic types - elastic, plastic, and penetration - and, as shown in figure 6, the shape of the signature is unique for each type. The acceleration and time scales of the plots in this figure are normalized: acceleration on the basis of the maximum acceleration encountered during impact and the time with respect to the total pulse time. The contact regions of the projectile and target corresponding to the different types are also included in this figure. The signature resulting from an elastic impact (fig. 6(a)) may be divided into two time intervals: the time of deformation during which the projectile comes to rest as the acceleration increases to its maximum value and as the two bodies deform and the time of restitution during which the motions of the bodies are reversed and they recover from their respective deformation. The figure shows that, in the case of perfectly elastic bodies, an axis of symmetry exists about the point of maximum deformation, thus, the integral under the acceleration-time curve is equal to twice the impact velocity for perfectly elastic impacts. However, since perfectly elastic impacts are never realized in practice, a more realistic case, unsymmetric about the point of maximum deformation owing to the partial restitution, is also shown. The impact of a steel projectile on concrete in the tests reported herein typifies a partially elastic type of impact, particularly for impacts of light projectiles at low velocities which result in little or no permanent deformation of either the projectile or target. Figure 5(a) presents a typical acceleration time history recorded during such an impact, and its resemblence to the elastic case of figure 6(a) is readily apparent.

The restitution increment of the impact signature vanishes in the event of a completely plastic impact as shown by figure 6(b). The area under the acceleration-time curve for this type of impact is equal to the impact velocity. This type of impact results in a permanent

L
1
6
7
0

deformation of either the target or the projectile or both as a result of the energy absorption capability of either or both bodies. Acceleration time histories recorded during the impact tests on lead and balsa targets (as shown in figs. 5(b) and 5(c)) appear to be analogous to the realistic plastic impact signature defined in figure 6(b).

The third type of impact encompasses those cases wherein the projectile passes through a portion of the target material to depths greater than the radius of the projectile. A representative signature for this type of impact (called penetration) is given in figure 6(c). The shape of this signature consists of a peak acceleration occurring almost immediately upon impact, an interval during which the acceleration slowly decreases as penetration takes place, and a rapid decrease in acceleration occurring at the time of complete penetration. The accelerations of the initial time interval are believed to be the result of the forces associated with the target inertia forces and the elastic forces associated with the rapid compression of the target material just ahead of the partially imbedded projectile which, upon expansion, forms the crater associated with such materials. The accelerations thereafter are primarily the result of forces exerted on the body during the penetration process - the drag or friction forces on the projectile caused by the shear and compressive forces exerted on the target material. Typical time histories of the accelerations resulting from this type of impact are presented in figures 5(d) to 5(h) for impacts on sand, soil, and several layer targets. The high-frequency component which appears in the signature recorded during impact on sand seems to be characteristic of impacts on granular materials and which arises, apparently, as a result of friction-like forces inherent in such target materials. Similar high-frequency components are present in the impact signatures of sod (when penetration depths were appreciable) and soil, which are apparently due to the high granular content of these targets. An additional characteristic, noted in the signatures recorded during impact in loose materials, is a double peak in the acceleration shown to occur in sand (fig. 5(e)) and in the dry portland cement portion of figure 5(f). In these cases, the second acceleration peak is believed to be the result of a substantial increase in the forces occurring during the penetration process which were found to be generally predominant for impacts in such materials. Two additional acceleration time histories of the penetration type are included in figure 5 to show the results of impact on targets consisting of layers of two different materials. The pulse shapes resulting from the impact of a projectile onto a layer of dry portland cement on soil (fig. 5(f)) and onto a layer of loose peat moss on balsa (fig. 5(h)), are shown to illustrate the ability of the acceleration-time-history technique to distinguish the layer characteristics of target materials. Just as in the case of the plastic type of impacts, no restitution is associated with the penetration type; hence, the impact velocity in all cases equals the area under the acceleration-time curve.

The shape of the signatures defines the type of impact; however, a physical description of these phenomena requires a knowledge of the acceleration and time scales such as given in figure 5. From a knowledge of these scales, the impulsive forces, jerk characteristics, and so forth can be readily evaluated from the impact signatures. Because of the large number of impact tests conducted, it was essential to obtain a convenient method of summarizing the data to permit the various impact signatures to be readily compared. Analysis of the data showed that a convenient way to obtain this summary would be to consider the magnitude of certain characteristics of these signatures. The characteristics chosen - the magnitude of the peak acceleration, the time required to reach that acceleration, and the total duration of the pulse - have been evaluated from the acceleration time histories obtained during the impact of the test projectiles on the various targets considered. These characteristics, together with the measured resulting crater dimensions, are presented as a function of the impact velocity or parameters composed of variables contained in available impact theories or developed from an empirical analysis of the experimental data.

L
1
6
7
0

Application of Available Theories

Numerous laws and theories have been developed for use in the field of impact to study and to explain various facets of the subject. An up-to-date and rather complete bibliography is given in reference 9. Many such laws have been considered nonapplicable in this study because of their limitations, boundary condition requirements, and/or cumbersome applications. Those theories or laws which were considered applicable to the reduction and analysis of the experimental data of this report, however, are referenced and discussed briefly in the sections that follow. In view of the differences which exist in the three general types of impact, as presented in the section entitled "General Discussion," the appropriate laws treating each of the three impact types are discussed in the following sections.

Elastic impacts.- The elastic type of impact phenomena received a classic treatment by H. Hertz who derived what is now known as the Hertz Law of Contact. This law is developed in reference 9 which cites the original treatise published in 1881. In this development, a solution was obtained in the form of a potential which describes the deformation and stresses in a region immediate to the contact point as a function of the geometric and elastic properties of the impacting bodies. This solution, in a form suitable for engineering use, yields an expression for the maximum force resisting impact F in terms of the static compression in both the projectile and the target. This expression is

$$F = k\alpha^{3/2} \tag{1}$$

where k is a constant defined by the geometric and elastic properties of the projectile and target, and α is the maximum relative compression of the bodies in collision. For the case of a spherical nose projectile impacting onto a massive plane surface, k and α are given by the following expressions:

$$k = \frac{2}{3} \frac{\sqrt{2D}}{\pi} \frac{1}{\delta_p + \delta_t}$$

$$\alpha = \left[\frac{15}{8} \frac{\pi V_i^2 \left(\delta_p + \delta_t\right) m}{\sqrt{2D}}\right]^{2/5}$$

From Newton's second law of motion, the peak acceleration associated with this force is given by

$$a = \left[\frac{125}{72\pi^2} \frac{DV_i^6}{m^2\left(\delta_p + \delta_t\right)^2}\right]^{1/5} \tag{2}$$

In addition, an expression for the duration of contact in terms of the geometric and elastic properties of the bodies is also obtainable from the Hertz law. This expression is

$$t_t = 5.208\left[\frac{\left(\delta_p + \delta_t\right) m}{\sqrt{DV_i}}\right]^{2/5} \tag{3}$$

Hence, through a knowledge of the geometric and elastic properties of two perfectly elastic bodies undergoing collision, the primary impact characteristics can be readily computed by means of the Hertz law. For the purposes of this paper, the impact of the test projectiles on concrete targets approximated an elastic type of collision; therefore, the experimentally measured peak accelerations and total pulse times are presented as a function of parameters contained in equations (2) and (3), respectively.

Plastic impacts.- In view of the restricted range of applicability of the Hertz law to perfectly elastic bodies, some efforts have been made to replace this law by a relation applicable to plastic contact

indentations. The relation which appears to be the most satisfactory, the Meyer law, also developed in reference 9 and more fully in reference 10, describes the indentation resulting from the impact of undeformable spherical nose projectiles onto softer plane surfaces in terms of the applied load or resisting force F. The basic assumption is made that the projectile is resisted by a flow pressure p in the target which is constant over the surface area of contact. In this case the relationship for the force is

$$F = \pi r^2 p \tag{4}$$

L
1
6
7
0

where r is the radius of the crater at the target surface. From the geometry of the indentation (fig. 6(b))

$$r^2 = \left(\frac{D}{2}\right)^2 - \left(\frac{D}{2} - y\right)^2$$

$$= Dy - y^2 \tag{5}$$

where D is the diameter of the projectile, and y is the penetration depth of the projectile into the target. With the assumption that the indentations are small relative to the projectile diameter, the relationship for the resisting force becomes

$$F = \pi p D y \tag{6}$$

Application of this relationship to the equation of motion yields

$$m \frac{d^2y}{dt^2} + \pi D p y = 0 \tag{7}$$

where m is the mass of the projectile. The solution of this equation, if it is assumed that $y = 0$ at $t = 0$ or that time is measured from the point of impact, is given by

$$y = V_i \sqrt{\frac{m}{\pi D p}} \sin \sqrt{\frac{\pi D p}{m}}\, t \tag{8}$$

where V_i is the impact velocity, and the maximum penetration

$$y = V_i\sqrt{\frac{m}{\pi Dp}} \tag{9}$$

occurs at

$$t_r = \frac{1}{2}\sqrt{\frac{\pi m}{Dp}} \tag{10}$$

Upon substitution of equation (9) into equation (6) and with application of Newton's second law of motion, the maximum acceleration during the impact is simply

$$a = V_i\sqrt{\frac{\pi Dp}{m}} \tag{11}$$

Therefore, for the case of the impact of a hard spherical nose projectile on a plastic-type target, the Meyer law permits the calculation of the maximum penetration of the projectile (eq. (9)) and the maximum acceleration (eq. (11)) in terms of the impact velocity, the projectile size and mass, and the dynamic flow pressure in the target. The Meyer law also permits the calculation of the time from the instant of impact to maximum acceleration by means of an expression (eq. (10)) which is dependent on the size and mass of the projectile and the dynamic flow pressure in the target material. Since this expression for rise time is independent of impact velocity, it is not, in this respect, significantly unlike the Hertz law for elastic impacts where the total pulse time is inversely proportional to the one-fifth power of the impact velocity.

The application of the Meyer law to plastic impacts appears to be limited to a range of penetration depths between approximately one-tenth and one-half the diameter of the projectile nose (ref. 10). The impact of the test projectiles on lead and balsa targets appeared to satisfy this limitation and to resemble plastic type of impacts; therefore, the penetration depths, peak accelerations, and corresponding rise times measured in these tests are presented as a function of parameters consisting of variables contained in the appropriate Meyer relationships. Except for the higher velocities, the impact of the test projectiles on sod targets yielded penetration depths which, in general, were within the depth limitations imposed by the Meyer law and yielded signatures which suggested plastic impacts. (At the higher velocities the impact signatures for this material became more indicative of penetration-type

impacts.) Therefore, the experimentally measured characteristics of impacts on sod are also presented as a function of the parameters taken from equations (9), (10), and (11).

Penetration impacts.- A great deal of experimental data has been collected over the years in an effort to explain the complicated mechanism of penetration. The present state of the knowledge consists primarily of empirical relationships based upon a variety of experimental observations. For example, references 9, 11, 12, and 13 arrived at empirical expressions for penetration depths of assorted projectiles into a wide variety of targets which have included such factors as projectile and target densities, sound speeds in both target and projectile, and the drag coefficients during penetration. However, all of these experimental observations give but a limited picture of the penetration process, valid for certain ranges of velocities, specific materials, and impact geometries. As such, it has not been possible to adequately describe the characteristics of penetration-type impacts.

L
1
6
7
0

It was felt in this study that in order to understand the characteristics of the impact of hard undeformable projectiles onto penetrable targets, such as soil and sand, the effects of several variables should first be studied. Tests were therefore conducted to evaluate the effects of impact velocity and the mass and diameter of the projectile on the resulting impact characteristics. From these tests, empirical expressions were formulated for each target material which relate the peak acceleration and penetration depth to these parameters. It should be pointed out that these expressions are subject to change when applied to other targets because of possible differences in the properties of the targets such as their composition, density, compactness, and so forth.

Low-Velocity Impact (5 to 30 fps)

Concrete.- The results of the experimental low-velocity-impact tests of the projectiles on deep concrete targets are presented in figures 7 to 10. In figure 7 the peak accelerations are presented as a function of a parameter composed of the variables contained in the Hertz expression for the peak accelerations of perfectly elastic impacts. The theoretical Hertz expression (eq. (2)) is also plotted in this figure for two combinations of μ and E for concrete: the average values as noted in reference 14 and values which were found to best fit the experimental data. The figure shows that the trend of variation of the experimental peak accelerations with the test variables (V_i, m, and D) agrees with that predicted by the Hertz law, but that the experimental peak accelerations are approximately 30 percent less than the accelerations predicted by the Hertz law with the use of average available values of E and μ for the target. Deviations of the experimental data for

the heavier projectiles from the trends predicted by the theory are attributed to a reduction in the measured peak accelerations resulting from local pulverization that occurs during impact of these projectiles on the concrete targets. (Accelerations predicted by Hertz are characterized by a complete recovery of any deformation following the impact.)

In addition to the peak acceleration, characteristic times were also measured from the acceleration time histories recorded during the impact of the test projectiles on concrete targets. The total pulse times of the various projectiles are averaged at each impact velocity and plotted as a function of a parameter composed of the variables in the corresponding theoretical expression for elastic impacts (eq. (3)) in figure 8. This figure shows that the experimental total pulse times are essentially independent of projectile diameter, are increased with increasing projectile mass, and appear to decrease slightly with increasing impact velocity over the range of these tests. The total pulse time, or duration of contact, as predicted by the Hertz law is also included in this figure and, using average E and μ properties of the target, appears to be applicable for the case of the light projectiles, but predicts total pulse times that are somewhat less than those measured experimentally for the heavier projectiles. However, application of the E and μ values which suited the expression for the peak accelerations permits the theoretical expression to predict more closely the total pulse times of the heavier projectiles.

No expression for the rise time, or time to reach peak acceleration, is given by the Hertz law; however, from the basic assumption of perfectly elastic impacts, which result in symmetrical acceleration time histories, the theoretical rise time is simply one-half the total pulse time. The experimentally measured rise times were averaged for the different projectiles at each of the test velocities and divided by the corresponding averaged total pulse times. This relationship, presented in figure 9 as a function of impact velocity, indicates that the lighter projectiles show rise times which are approximately one-half the total time which agrees favorably with the Hertz law and is indicative of an elastic impact. (See fig. 6(a).) The projectiles of higher mass show ratios less than 1/2 which verifies the experimental observations that conditions were not commensurate with purely elastic type impacts.

Further evidence illustrating that the heavier projectiles do not exhibit the purely elastic characteristics of the lighter projectiles impacting concrete targets is afforded by the restitution velocities of figure 10. These velocities (averaged for the different projectiles at each impact velocity) were obtained by subtracting the known impact velocities from the values determined from an integration of the acceleration time histories recorded during impact. These differences, which represent the restitution velocities, are presented in the figure as a

ratio to the corresponding impact velocity. The data show that the impact of the heavier projectiles results in restitution velocities which are about 31 percent of the corresponding impact velocities over the velocity test range. On the other hand, the lighter projectiles showed restitution velocities as high as 48 percent of the impact velocities. This difference in restitution is indicative of the energy absorbed in pulverizing the target during the impact of the heavy projectiles. It is also apparent from the trends of the restitution velocities in the figure that the two smaller light projectiles pulverize the target at the higher impact test velocities.

L
1
6
7
0

Lead.- The impact characteristics of the test projectiles on lead targets are presented and compared, when possible, with available theory in figures 11 to 14. The peak accelerations and characteristic times, both obtained from acceleration time histories recorded during impact, are given in figures 11 to 13 and penetration depths are presented in figure 14.

The impact of the test projectiles on lead targets develop shallow permanent deformations in the target accompanied by a minimum of elastic effects (restitution) which suggests plastic-type impacts and the applicability of the Meyer law. Therefore, the experimental peak accelerations are presented as a function of the parameter $V_i\sqrt{D/m}$ obtained from the Meyer expression for peak acceleration in plastic impacts (eq. (11)). Since the data, when plotted on this basis, may be represented by one curve (fig. 11), a unique relationship exists between the peak accelerations and this parameter. The figure shows that the peak acceleration varies directly with this parameter and the Meyer expression, based upon a dynamic flow pressure of 13,000 lb/sq in., predicts the maximum accelerations encountered during the low-velocity-impact tests of the projectiles on lead targets. This value of dynamic flow pressure is in good agreement with that obtained experimentally in reference 15 at impact velocities up to 2 feet per second. However, in applying the Meyer law to other characteristics measured during impact on lead targets, a dynamic flow pressure of 21,000 lb/sq in. appeared to best fit the experimental data; therefore, for the sake of completeness the theoretical peak acceleration based upon this dynamic flow pressure is also included in figure 11.

The experimental rise times obtained from the signatures recorded during impact of the projectiles on lead targets are averaged at each impact velocity and presented in figure 12 as a function of a parameter composed of the variables in the corresponding theoretical expression for plastic impacts (eq. (10)). In addition, the theoretical expression for rise times, based upon a dynamic flow pressure of 21,000 lb/sq in., is also included in this figure. The figure shows that the experimental

rise times for the heavier projectiles are independent of the impact velocity, as suggested by the theory, and agree with the times predicted by the theory. The experimental rise times for the lighter projectiles, however, differ slightly from the theory. In these cases the theory predicts rise times that are somewhat higher than those obtained experimentally. In addition, the experimental times tend to decrease with increasing impact velocity in a manner similar to that predicted by the Hertz law which suggests possible elastic effects. Figure 13 shows the effect of projectile diameter and projectile mass on the ratio of the rise time to total pulse time measured experimentally during the impacts on lead targets. The data points on this figure represent the ratio of the average times measured at each test velocity for the different projectiles. The figure shows that this ratio is decreased with increasing projectile diameter and, for the lighter projectiles, is decreased with increasing test velocity. The effect of projectile mass appears insignificant. This figure indicates that the impact of the test projectiles on lead targets is of the plastic type (with possibly some elastic effects included) since the average ratio of rise time to total pulse time is approximately 6/10, a figure compatible with such impacts. (See fig. 6(b).)

As previously stated, the Meyer law also gives an expression for determining penetration depths resulting from plastic-type impacts. This expression (eq. (9)) is presented in figure 14 for purposes of comparison with the experimentally measured depths. In this figure the penetration depth is plotted as a function of a parameter consisting of the test variables as contained in the theoretical expression. The figure shows that the theory, based upon a dynamic flow pressure of 21,000 lb/sq in., compares well with the experimental data.

Balsa.- The impact of the projectiles on balsa targets is not strictly plastic in nature because of the elasticity inherent in these targets when the balsa fibers are not sheared by the projectiles. The application of the Meyer law for plastic impacts on these targets is complicated by this fact, particularly at low impact velocities where the balsa fibers appear to remain intact. On the other hand, the application of the Hertz law for elastic impacts is invalid since a permanent deformation exists following the impact of projectiles at all velocities. Nevertheless, since it seemed to be the most appropriate method available for analyzing the impact characteristics of the test projectiles on balsa targets, the Meyer law was used whenever possible and compared with the results of the experimental low-velocity-impact tests in figures 15 to 19. In other cases, notably for penetration depths, empirical relations are given.

The elastic properties of balsa are illustrated in figure 15 where the average restitution velocity for each projectile is divided by the corresponding impact velocity and plotted as a function of that impact velocity. This figure shows that the restitution velocities are

insensitive to changes in the projectile mass but decrease with both increasing impact velocity and decreasing projectile diameter. Such evidence of elasticity in the target indicates that the measured penetration depths of these projectiles would be somewhat less than the maximum penetrations actually attained during impact and suggests that the Meyer expression for penetrations is not adequate.

An empirical analysis of the experimental penetration depths resulting from impact on balsa targets indicates that the expression

$$y = 0.12V_i \frac{m^{3/4}}{D^2}$$

L
1
6
7
0

describes the penetration depths in terms of the test variables. This expression was obtained from the curve that best fits the experimental data of figure 16 where the penetration depths are plotted as a function of $V_i \frac{m^{3/4}}{D^2}$. Since this expression is significantly different from that given by the Meyer law where

$$y = V_i\sqrt{\frac{m}{\pi Dp}}$$

it is evident that the Meyer law is incapable of predicting the penetration depths in balsa targets.

The experimental peak accelerations, presented in figure 17 as a function of the test variables as contained in the Meyer expression for peak acceleration, show fair agreement with the Meyer law when a constant flow pressure of 180 lb/sq in. is assumed for balsa. It appears from the data as presented in the figure that the Meyer law predicts the variations of peak acceleration with respect to impact velocity but slight deviations exist for variations with respect to projectile mass and diameter.

The experimental rise times measured for the different projectiles impacting balsa targets were averaged at each impact velocity and are presented in figure 18 as a function of a parameter obtained from the corresponding theoretical expression for plastic impacts as given by equation (10). This equation, resulting from the Meyer law, is also plotted in the figure for a dynamic flow pressure of 435 lb/sq in. which appears to best fit the experimental test data. The figure shows that the variation of the measured rise times with projectile mass and diameter agrees with that predicted by the Meyer law, and the magnitudes of

the experimental rise times are in accord with the theoretical times based upon this value of dynamic flow pressure. Although the theory states that the rise times are independent of impact velocity in this target, the experimental rise times, as shown by the data, appear in general to decrease slightly with increasing impact velocity.

The ratios of the measured rise times to the measured total pulse times (given in fig. 19 for impacts on balsa) do not appear to be indicative of plastic-type impacts. Values of this ratio, between 0.4 and 0.5, are inconsistent with values expected from such impacts. (See fig. 6(b).) This inconsistency can be explained by an examination of a typical acceleration time history recorded during impact in balsa such as given in figure 5(c). This figure shows that the initial portion of the restitution period is typical of plastic impacts but the final portion differs in that it consists of a long low acceleration period rather than immediately returning to zero acceleration. This final portion of the restitution period is necessarily included in the measured total pulse times and is reflected in the correspondingly small time ratios of figure 19.

Sod.- As previously stated, the low-velocity impacts of the test projectiles on sod targets were generally plastic in nature; therefore, the experimentally measured impact characteristics are presented, when possible, as a function of the parameters taken from appropriate Meyer law expressions. These characteristics of sod are presented in figures 20 to 23 and are compared with the available corresponding Meyer expressions as given in equations (11), (9), and (10). As in the case of impacts on the other basically plastic targets, lead and balsa, the variation of peak acceleration and average rise time with the test variables agrees with those predicted by the Meyer law. Furthermore, as was the case for lead and balsa, the dynamic flow pressure necessary to best fit these data by means of the appropriate Meyer law expression differs for the two impact characteristics. Whereas a dynamic flow pressure of 37 lb/sq in. permitted the Meyer law to predict the magnitude of the peak acceleration (fig. 20), a pressure of 130 lb/sq in. in the expression for rise time appears to best predict that characteristic (fig. 21). The rise times for the heavier projectiles are somewhat less than those predicted, on the basis of this dynamic pressure, by the Meyer expression which suggests that either the dynamic flow pressure of sod should be even greater than 130 lb/sq in. or that the impacts for these projectiles are not completely plastic in nature. It was observed from the acceleration time histories of these heavier projectiles that the impacts, particularly for the high-velocity cases, were definitely of the penetration type.

The ratios of the measured rise times to the measured total pulse times as given in figure 22 suggest that none of the projectile impacts were truly plastic because of the low values of this ratio (0.35 to 0.45).

These low values, however, were primarily the result of the total pulse times which, as in the case of balsa, consisted of restitution regions (see the impact signature of fig. 5(d)) which were characterized by a long low acceleration period rather than a rapid decrease to zero acceleration which normally defines the restitution region in plastic types of impact.

The Meyer expression for penetration depths (eq. (9)) is compared in figure 23 with the experimental measurements of this characteristic resulting from impacts in sod targets. The figure shows that the experimental data are in fair agreement with the theory when a constant flow pressure of 130 lb/sq in. is assumed for sod. Fluctuations in the experimental data are attributed to local differences in the sod targets.

L
1
6
7
0

Sand.- The accelerations measured from the multiple peak acceleration time histories recorded during the impact of the projectiles in loose No. 000 sand are plotted in figure 24. Also included in this figure are the empirical expressions derived from the experimental data. These expressions:

$$a_A = 1.24 \times 10^{-3} \frac{D^{5/3} V_i^{5/3}}{m}$$

and

$$a_B = 23.16 \frac{D^{4/3} V_i}{m^{2/5}}$$

relate the peak accelerations to the impact velocity and the significant projectile parameters. The figure shows that the empirical expressions appear to describe satisfactorily these peak accelerations. It was observed that within the velocity range of these tests, the second peak acceleration was always the greater except for the lighter projectiles impacting at the highest test velocity.

The times required to reach these acceleration peaks $t_{r,A}$ and $t_{r,B}$ are averaged at each impact velocity in figure 25 and divided by the total pulse times in figure 26. Because, in some cases the magnitude of the high-frequency components, referred to earlier, rendered the desired time characteristics doubtful, these data were not included in these figures.

Penetration depths of the projectiles impacting sand are presented in figure 27 and are shown to be described by the empirical expression,

$$y = 2.6 \frac{m^{1/2} V_i^{2/3}}{D}$$

The impact of the projectiles on sand afforded an additional impact characteristic which, because of its possible application in the design of vehicles intended to impact such media, is felt to be of significance. This characteristic, the diameter of the resulting blast crater, is divided by the projectile diameter and presented as a function of impact velocity in figure 28. The data of this figure show that this ratio is independent of the projectile mass, but is increased with increasing impact velocity and decreasing projectile diameter.

High-Velocity Impact (190 to 900 fps)

In an effort to establish techniques which would permit the evaluation of the impact characteristics over an extended velocity range, high-velocity tests were conducted with 3-inch-diameter projectiles at velocities up to 900 fps. The high velocities of the projectiles were obtained by means of the air gun shown in figures 3 and 4. In the course of these tests, two projectile parameters - mass and nose shape - were examined to determine their effect on the resulting impact characteristics.

Acceleration time histories were obtained in these tests at impact velocities up to 225 fps (fig. 5(g)) by means of trailing wire circuitry. Peak accelerations, however, were obtained at all velocities by means of copper-ball accelerometers which were also mounted within the projectiles. The peak accelerations measured during these high-velocity-impact tests are presented in figure 29 and compared with an empirical expression derived from an analysis of the experimental data. This expression

$$a = 6.18 \times 10^{-2} \frac{V_i^{3/2}}{m}$$

appears to adequately describe the peak accelerations measured during impact in soil, irrespective of the two nose configurations examined.

The measured penetration depths resulting from high-velocity impact of projectiles having different mass and nose configurations in soil are presented in figure 30 as a function of an experimentally obtained

empirical expression for the depths. The figure shows that this expression

$$y = 0.005mV_i^{3/2}$$

describes the penetration depths and indicates that the penetrations are independent of the nose configurations examined.

L
1
6
7
0

Application of Results

The characteristics of the acceleration time histories include the magnitude of the peak acceleration, the time required to reach that acceleration, the total duration of the pulse, and the pulse shapes which are associated with the nature of the projectile and the target. These characteristics have been evaluated from the acceleration time histories obtained during the low-velocity-impact tests of a variety of projectiles onto several different targets. In addition, theoretical and empirical expressions are available which relate these characteristics to properties of the projectile and the target. However, these expressions are only applicable to a given target material and a more general expression for these characteristics, accommodating all the target materials, would be useful in defining the characteristics of any unknown target. A consideration of the theoretical expressions for certain of these characteristics resulting from elastic and plastic impacts reveals that relationships are available which are independent of the physical and geometric properties of both projectiles and targets. From the Hertz law for elastic impact, the product of the expressions for peak acceleration (eq. (2)) and total pulse time (eq. (3)) yields the relationship

$$a = 3.68 \frac{V_i}{t_t}$$

A similar expression results from the product of equations (10) and (11) for plastic impacts; this expression is

$$a = 1.57 \frac{V_i}{t_t}$$

These expressions, based upon perfectly elastic and perfectly plastic impacts $\left(t_r = t_t \text{ in a perfectly plastic impact}\right)$, have numerical

coefficients that differ. In practice, however, neither perfectly elastic nor perfectly plastic impacts would be realized and in an effort to obtain a more realistic coefficient - one possibly applicable to both types of impact - the experimental measurements of these two characteristics are presented in figure 31. In this figure, the ratio of the peak acceleration to the corresponding impact velocity (averaged at each test velocity) is plotted as a function of the total pulse time for impacts onto all target materials. Projectiles and targets are both identified on the figure. Although the impacts on sand were neither elastic nor plastic in nature, the results of tests on this material, including both accelerations of the multiple peak signatures, are also given. The data of this figure are best fitted by the expression

L
1
6
7
0

$$a = 2.1 \frac{V_i}{t_t}$$

which, in relating the peak acceleration to the total pulse time for all test projectiles and targets, differs only from the theoretical relationships by the numerical coefficient. This figure shows that the magnitude of the peak acceleration and the total pulse time is dependent upon the target material. This fact is better illustrated in figure 32 where the data of one projectile (taken from fig. 31) are again presented, together with the faired curve. The targets associated with these data are indicated in the figure and it is clearly shown that the magnitudes of the peak accelerations and total pulse times are related to the target material. The data for these targets occupy definite positions along the faired curve which appear to follow a sequence suggesting that the magnitudes of the peak accelerations and total pulse times are indicative of the resistance of the target material to penetration or target hardness. Thus, it appears that, for a given projectile, positions along the curve for peak acceleration against total pulse time can be defined for materials having a wide hardness spectrum which may be considered as an accelerometer-response—target-hardness calibration for the given projectile.

The data of figures 31 and 32 show that useful information on the hardness or penetrability of a target material may be obtained if a measure of either the peak acceleration during impact or the corresponding total pulse time is known. A knowledge of both would, of course, insure the results. With the additional knowledge of the pulse shape, the impact may be further classified as to type and provide sufficient information to adequately describe the nature of the target. Such information is provided by a complete impact acceleration time history, knowledge of which would be required in evaluating the hardness of a remote surface, such as the moon.

CONCLUSIONS

The impact of the various test projectiles on the different target materials produced acceleration time histories which contain several significant characteristics. These characteristics include the pulse shape, the magnitude of the peak acceleration, the time required to reach that acceleration, and the total duration of the pulse. The results of a study to evaluate these and other related impact characteristics suggest the following conclusions:

L
1
6
7
0

1. The shape of the acceleration time history is unique for each of the three general types of impact - elastic, plastic, and penetration - and is capable of distinguishing the layer characteristics of certain target materials.

2. The variation of the experimental peak accelerations and characteristic pulse times with the test variables (impact velocity, projectile mass, and diameter) agrees, in general, with that predicted by the Hertz law for elastic impacts and by the Meyer law for plastic impacts. The magnitudes of the experimental peak accelerations for impact on concrete are approximately 30 percent less than those theoretically predicted for perfectly elastic impacts, based upon average available values of modulus of elasticity and Poisson's ratio for concrete. The total pulse times predicted by the Hertz law, based upon average properties of modulus of elasticity and Poisson's ratio for concrete, appears to be applicable for the case of the light projectiles, but are somewhat less than those measured experimentally for the heavier projectiles. Two values of the dynamic flow pressure are required to correlate the Meyer law with the experimental data for plastic impacts. In all impacts of this type, the value required to predict peak acceleration is somewhat less than that necessary to predict penetration depths and characteristic times.

3. Empirical expressions were formulated from the experimental results obtained from penetration impacts which relate the peak acceleration and penetration depth to parameters containing the test variables. As in elastic and plastic impacts, the peak accelerations, measured from penetration impacts, increased with increasing impact velocity and projectile diameter and decreasing projectile mass. Furthermore, as one would expect, an increase in penetration depth results from increased projectile mass and impact velocity and decreased projectile diameter.

4. It appears from a comparison of the magnitudes of certain of these characteristics resulting from impact in all target materials, that a relative penetrability or hardness scale can be established. From such a scale, the surface hardness of a remote target, such as the moon, may be described in terms of the hardness of accessible earth

materials by comparing the acceleration time histories measured during impact of projectiles on the lunar surface with those of identical projectiles during impacts on known earth materials.

Langley Research Center,
National Aeronautics and Space Administration,
Langley Station, Hampton, Va., March 19, 1962.

L
1
6
7
0

REFERENCES

1. Anon.: Penetration of Projectiles Into Concrete, Rock, and Soil. Ch. 3 of Textbook of Air Armament, Pt. I, British Air Ministry, Feb. 1949. (Available from ASTIA as AD No. 145925.)

2. Sanford, Robert B.: Penetration Properties of Inert 500 lb GP Bombs Dropped on Sand. AFAC Tech. Rep. 53-54, Air Res. and Dev. Command, Dec. 1953. (Available from ASTIA as AD 23962.)

3. Kinard, William H., Lambert, C. H., Jr., Schryer, David R., and Casey, Francis W., Jr.: Effect of Target Thickness on Cratering and Penetration of Projectiles Impacting at Velocities to 13,000 Feet Per Second. NASA MEMO 10-18-58L, 1958.

4. Summers, James L.: Investigation of High-Speed Impact: Regions of Impact and Impact at Oblique Angles. NASA TN D-94, 1959.

5. McKenzie, R. J., Martin, F. F., and Kenworthy, H. M.: High Velocity Impact of Small Metal Spheres Upon Flat Metal Targets. Proc. Third Symposium on Hypervelocity Impact, vol. 1, F. Genevese, ed., Armour Res. Foundation, Illinois Inst. Tech., Feb. 1959, pp. 247-261.

6. Kinard, William H., and Collins, Rufus D., Jr.: An Investigation of High-Velocity Impact Cratering Into Nonmetallic Targets and Correlation of Penetration Data for Metallic and Nonmetallic Targets. NASA TN D-726, 1961.

7. Lang, H. A.: Lunar Instrument Carrier - Landing Factors. U.S. Air Force Project RAND Res. Memo. RM-1725 (ASTIA Doc. No. AD 112403), The RAND Corp., June 4, 1956.

8. Stathopoulos, G., and DeVost, V. F.: NOL Copper-Ball Accelerometers. NAVORD Rep. 6638, U.S. Naval Ord. Lab. (White Oak, Md.), May 6, 1959.

9. Goldsmith, Werner: Impact. Edward Arnold (Publ.) Ltd. (London), c.1960.

10. Tabor, D.: The Hardness of Metals. The Clarendon Press (Oxford), 1951.

11. Allen, William A., Mayfield, Earle B., and Morrison, Harvey L.: Dynamics of a Projectile Penetrating Sand. NAVORD Rep. 5823, U.S. Naval Ord. Test Station (China Lake, Calif.), Jan. 21, 1958.

L
1
6
7
0

12. Huth, J. H., Thompson, J. S., and Van Valkenburg, M. E.: A New Approach to Penetration Mechanics. [Paper] P-746, The RAND Corp., Oct. 6, 1955.

13. Rinehart, John S.: Stresses Associated With Lunar Landings. Contribution No. 11, Mining Res. Lab., Colorado School of Mines, Feb. 27, 1960.

14. Murphy, Glenn: Properties of Engineering Materials. Second ed., Int. Textbook Co. (Scranton, Pa.), c.1947, p. 393.

15. Crook, A. W.: A Study of Some Impacts Between Metal Bodies by a Piezo-Electric Method. Proc. Roy. Soc. (London), ser. A, vol. 212, no. 1110, May 7, 1952, pp. 377-390.

L
1
6
7
0

Configuration	m, lb-sec^2/in.	D, in.
1	0.0025	1
2	.0025	2
3	.0025	4
4	.0104	2
5	.0204	2

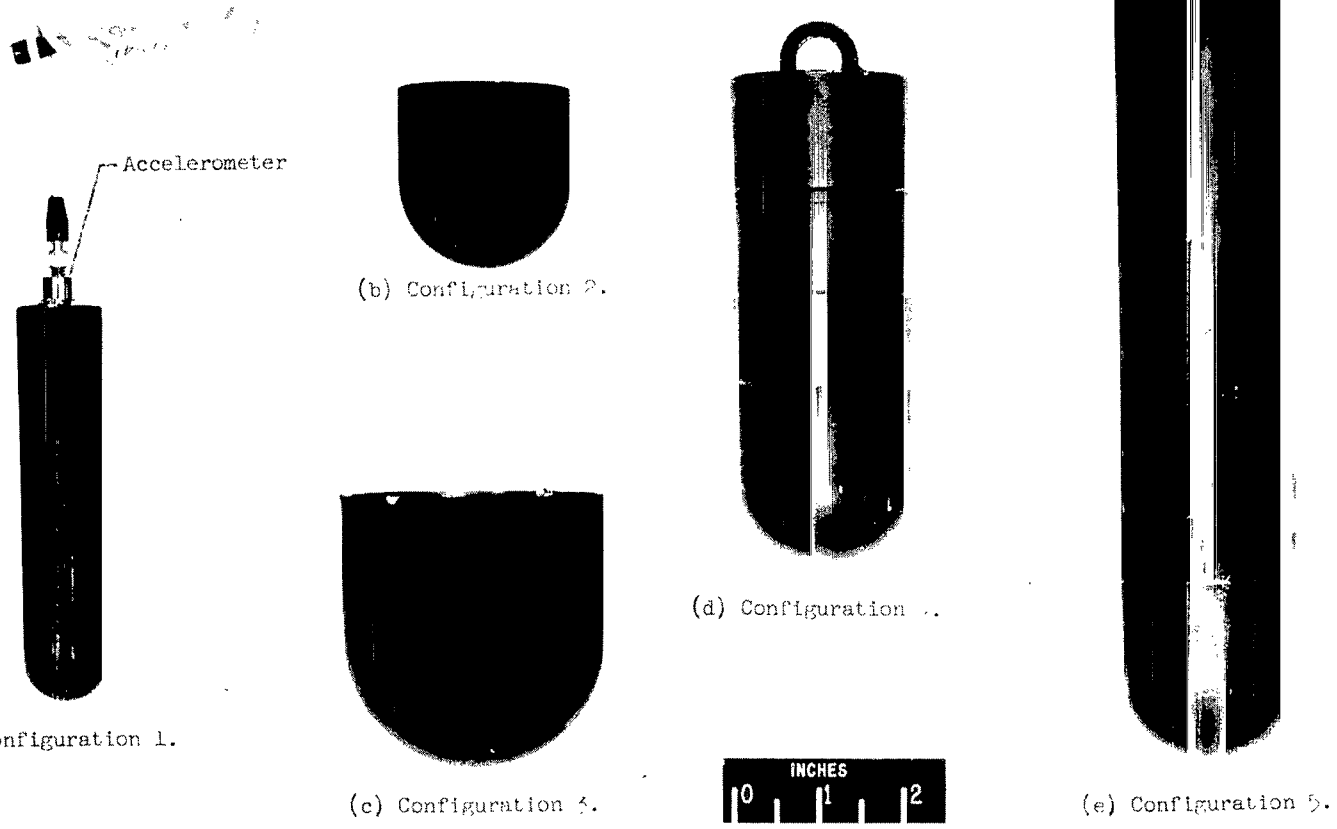

(a) Configuration 1.

(b) Configuration 2.

(c) Configuration 3.

(d) Configuration 4.

(e) Configuration 5.

Figure 1.- Projectile configurations for low-velocity-impact tests. L-62-56

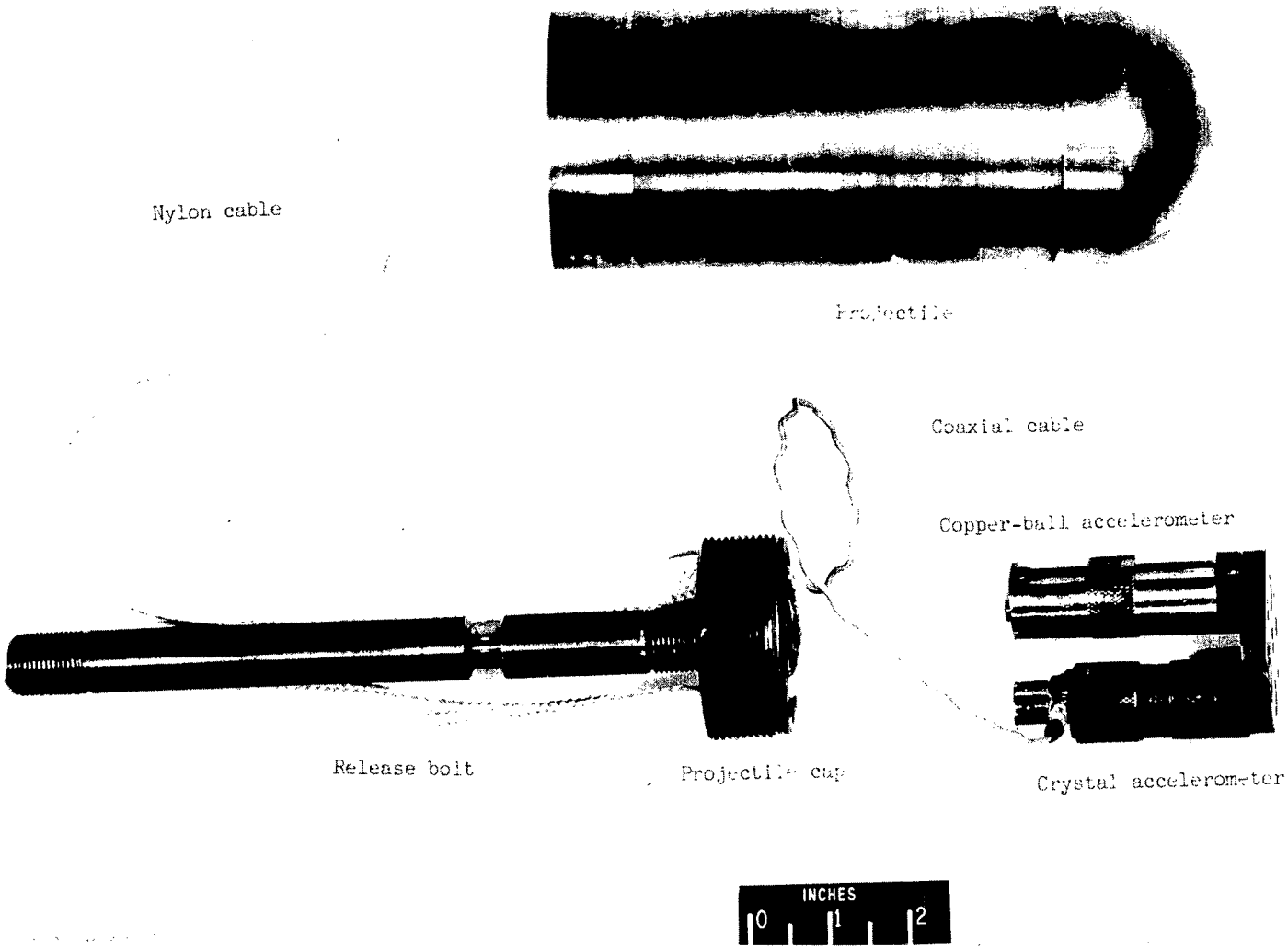

Figure 2.- Typical high-velocity-impact projectile and components. L-61-5959.1

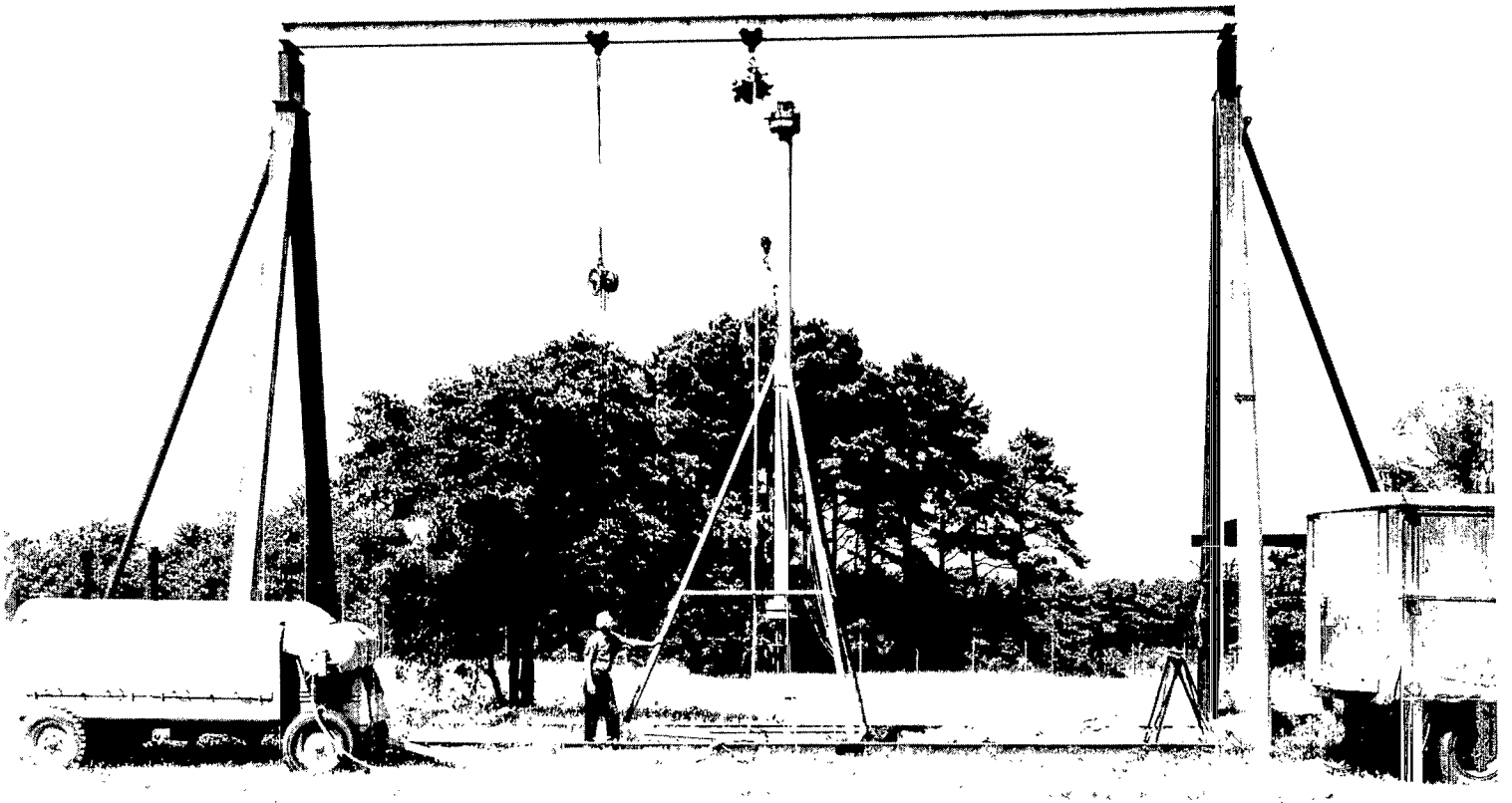

Figure 3.- Air gun and hoisting apparatus for high-velocity-impact tests. L-61-5641

L-1670

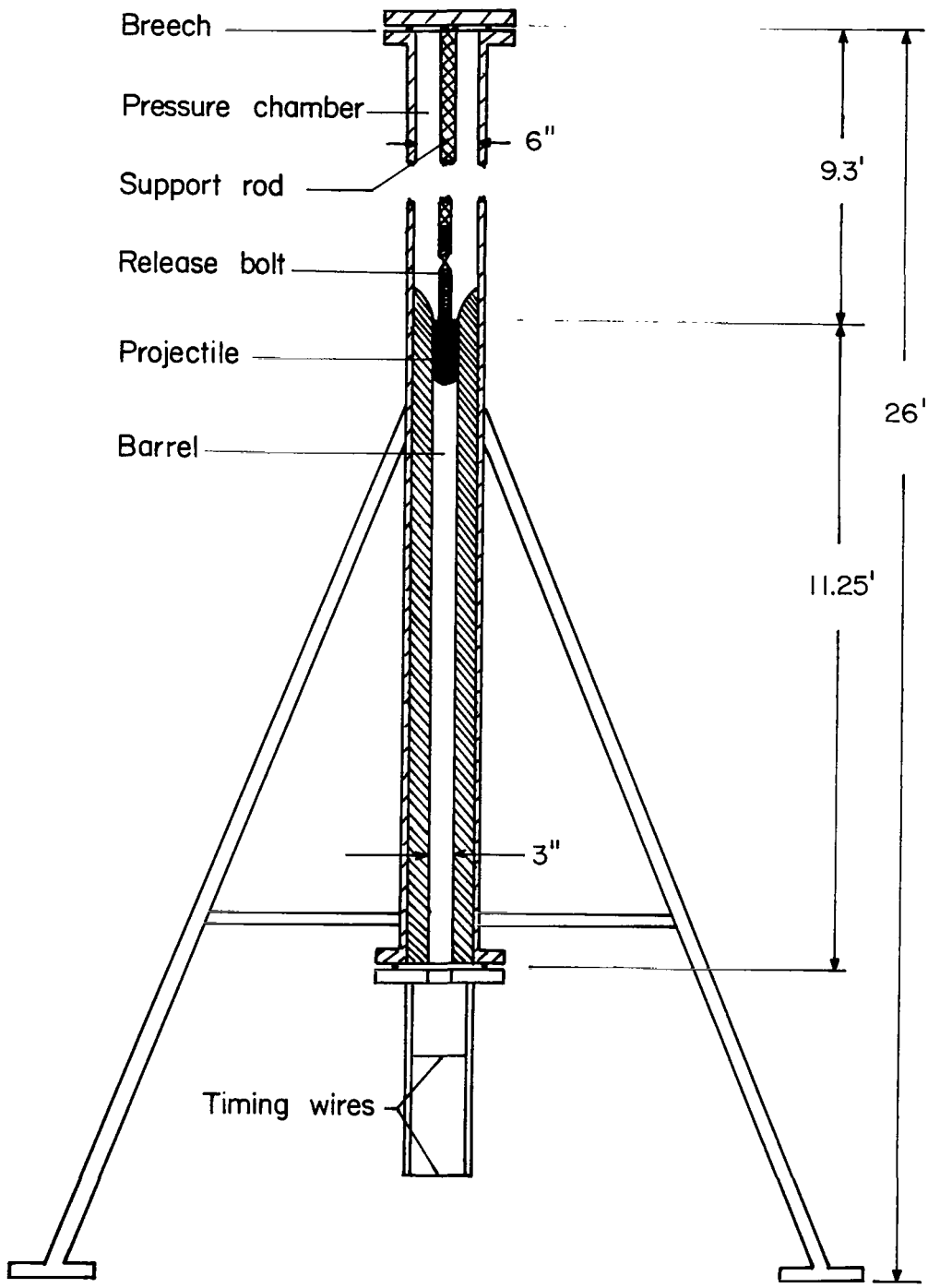

Figure 4.- Sectional sketch of air gun showing pertinent components and dimensions.

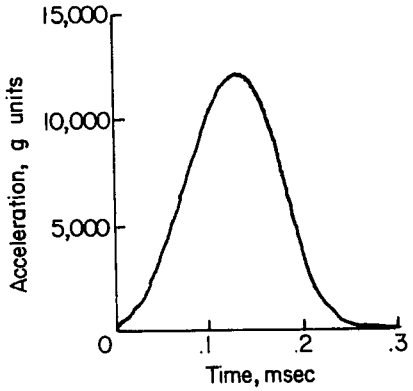

(a) Concrete; V_i = 30 fps; m = 0.0025 lb-sec^2/in.

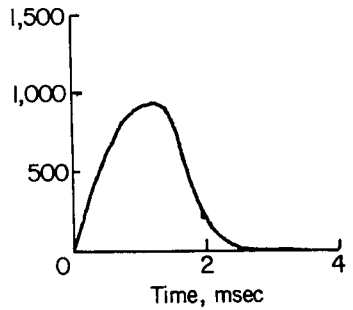

(c) Balsa; V_i = 30 fps; m = 0.0025 lb-sec^2/in.

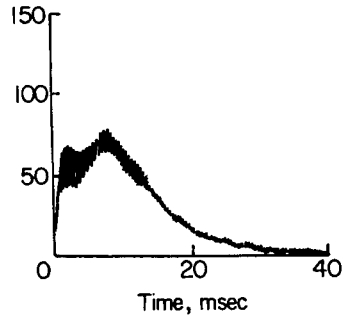

(e) Sand; V_i = 20 fps; m = 0.0025 lb-sec^2/in.

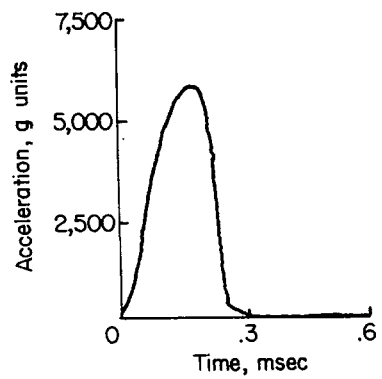

(b) Lead; V_i = 30 fps; m = 0.0025 lb-sec^2/in.

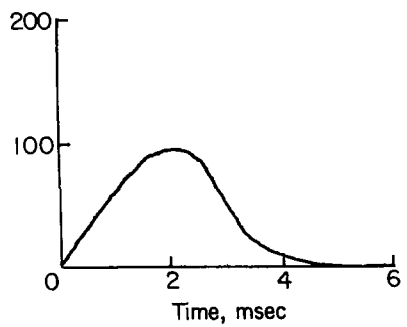

(d) Sod; V_i = 10 fps; m = 0.0025 lb-sec^2/in.

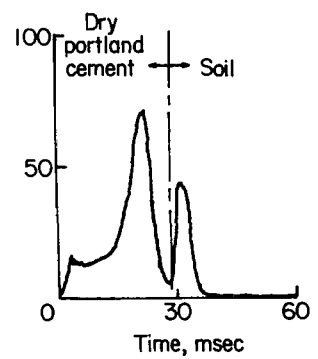

(f) Layer; V_i = 36 fps; m = 0.009 lb-sec^2/in.

Figure 5.- Reproduced samples of acceleration time histories recorded during impact of projectiles on different target materials. D = 3 inches.

L-1670

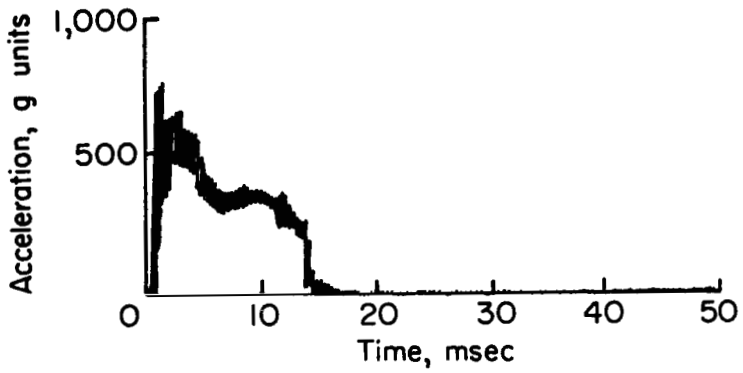

(g) Soil; V_i = 220 fps;
m = 0.022 lb-sec^2/in.

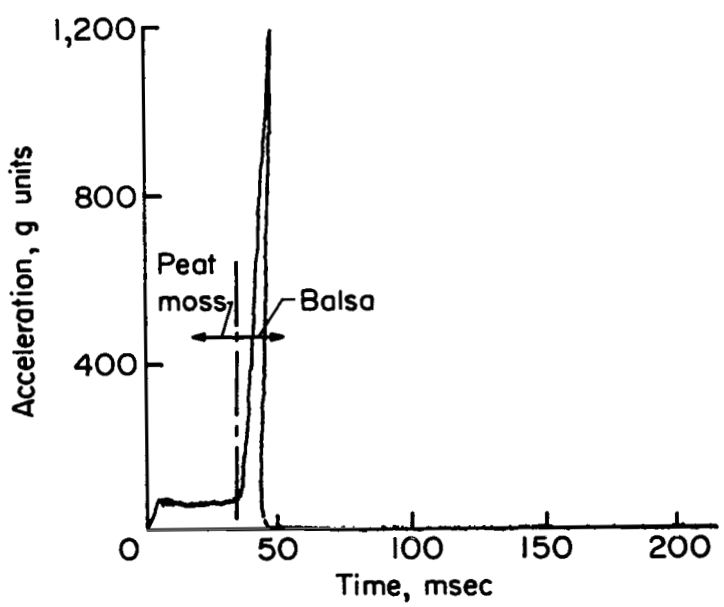

(h) Layer; V_i = 170 fps;
m = 0.009 lb-sec^2/in.

Figure 5.- Concluded.

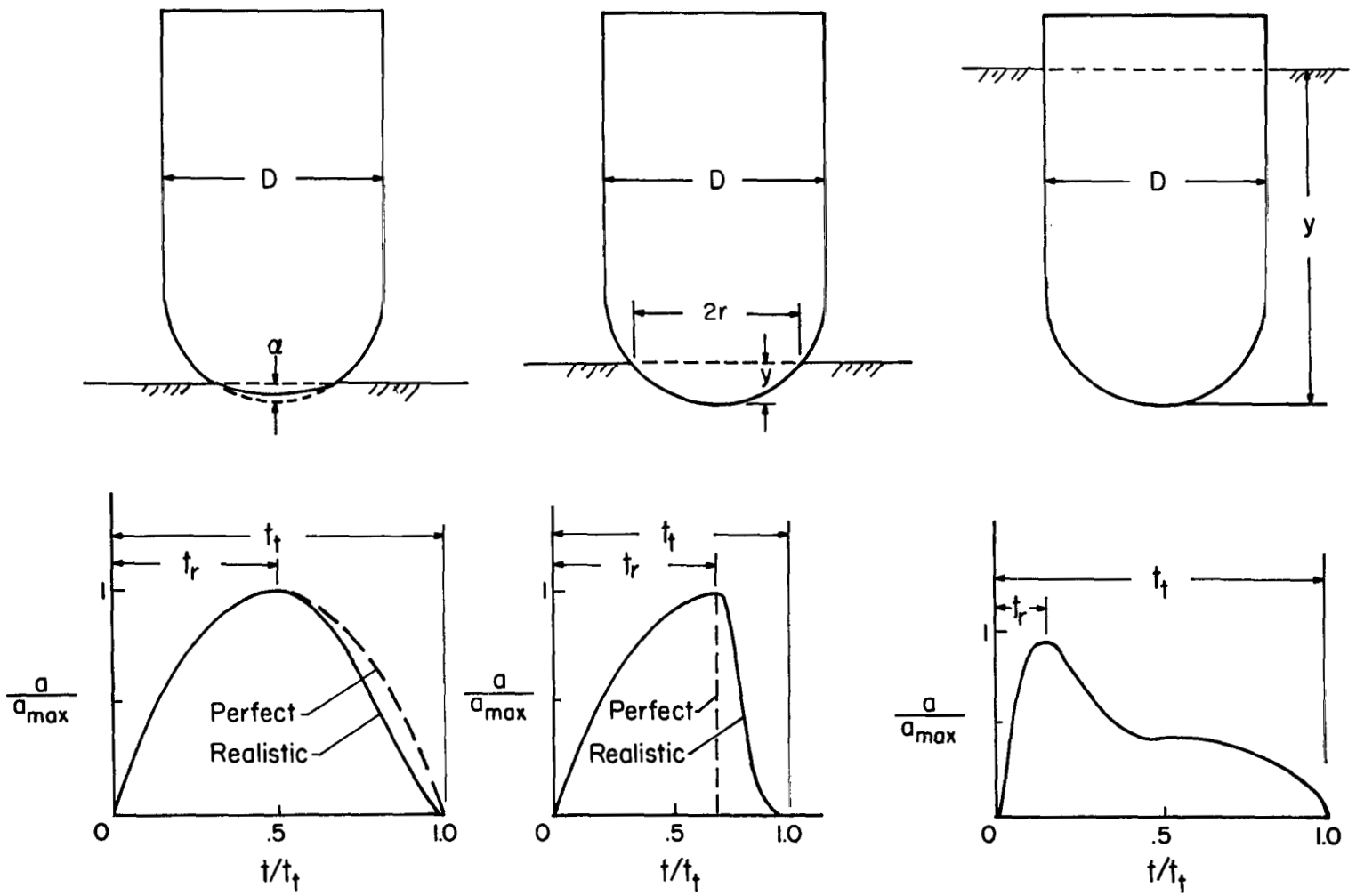

(a) Elastic. (b) Plastic. (c) Penetration.

Figure 6.- Sketch of acceleration time histories and contact regions for different impact types.

L-1670

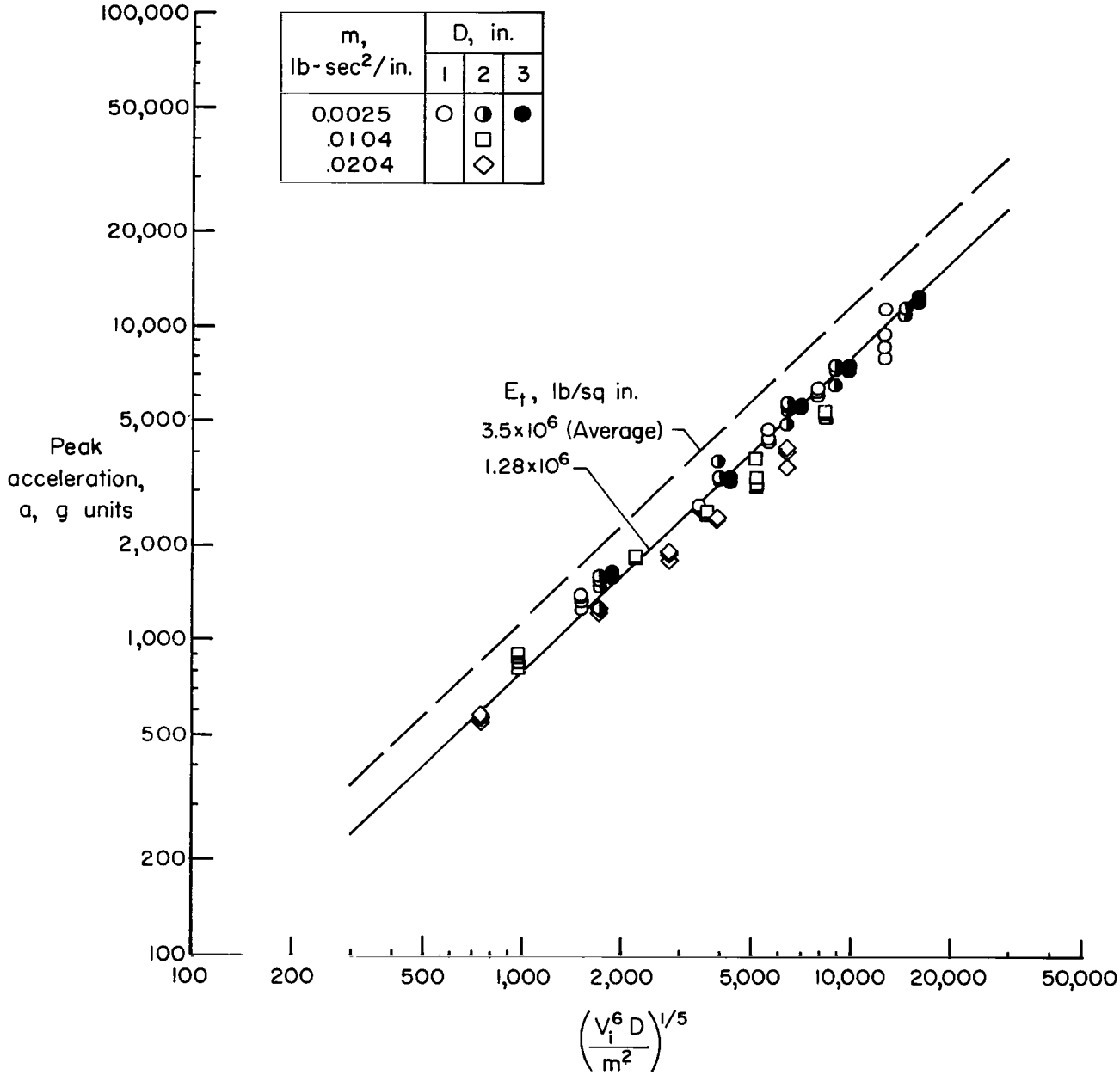

Figure 7.- Experimental and theoretical peak accelerations for impact of projectiles on concrete targets. $a = \left[\frac{125}{72\pi^2(\delta_p + \delta_t)^2} \frac{V_i^6 D}{m^2}\right]^{1/5}$; $\mu_t = 0.2$.

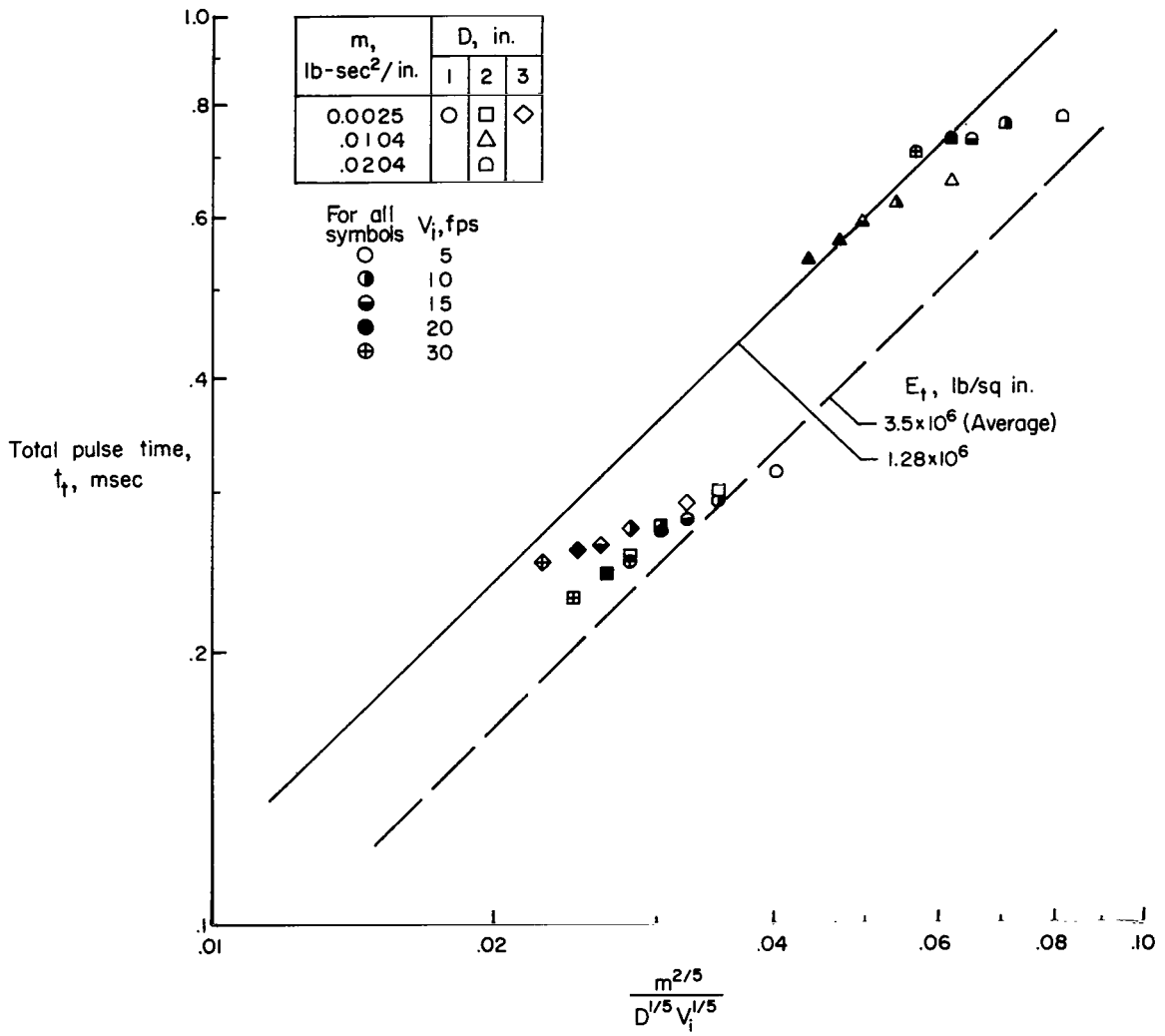

Figure 8.- Experimental and theoretical total pulse times for impact of projectiles on concrete targets. $t_t = 5.208\left[\frac{(\delta_p + \delta_t)m}{\sqrt{D}\ V_i}\right]^{2/5}$; $\mu_t = 0.2$.

L-1670

L-1670

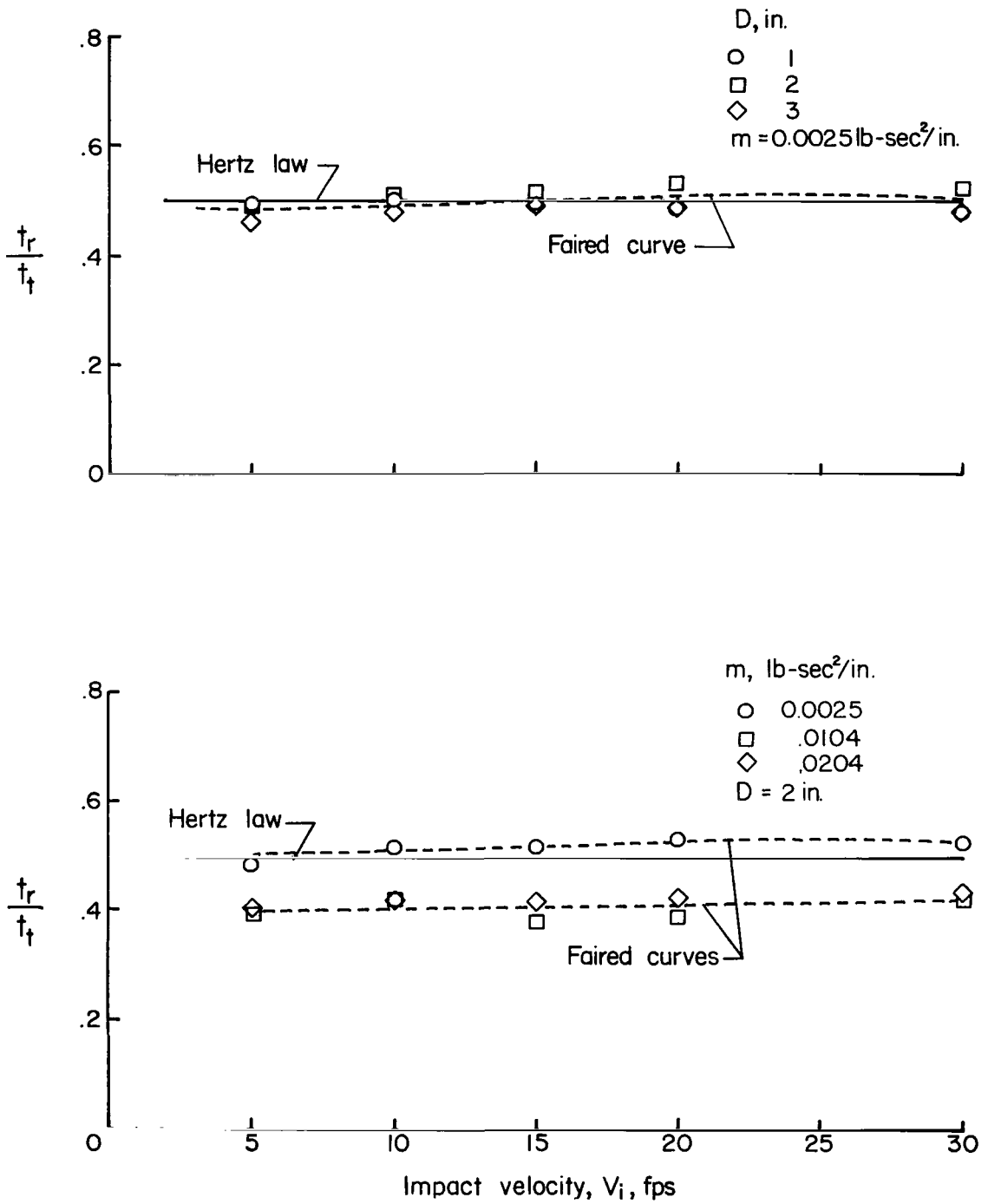

Figure 9.- Effect of projectile diameter and mass on characteristic times of impacts on concrete targets.

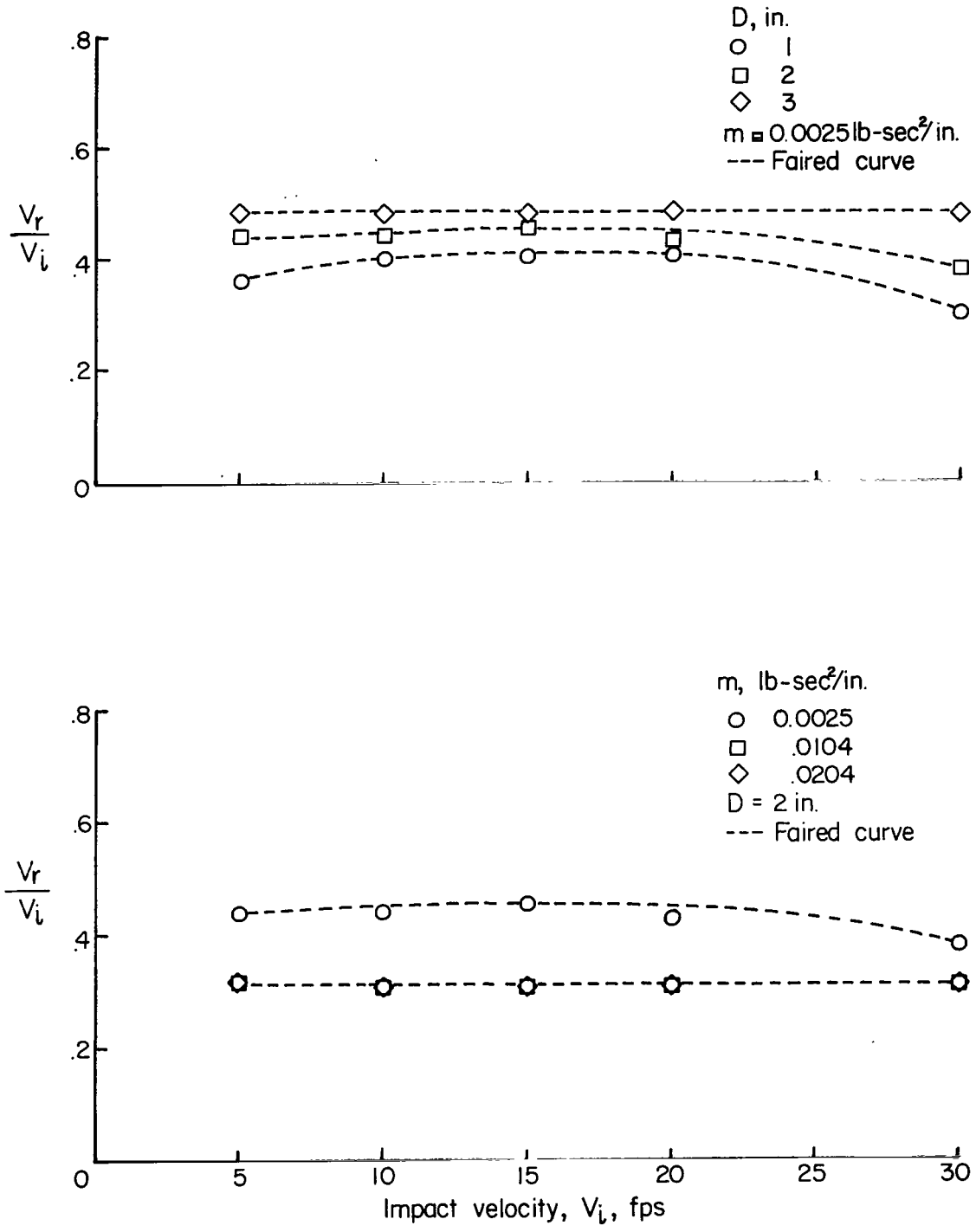

Figure 10.- Effect of projectile diameter and mass on restitution velocities measured during impact on concrete targets.

L-1670

L-1670

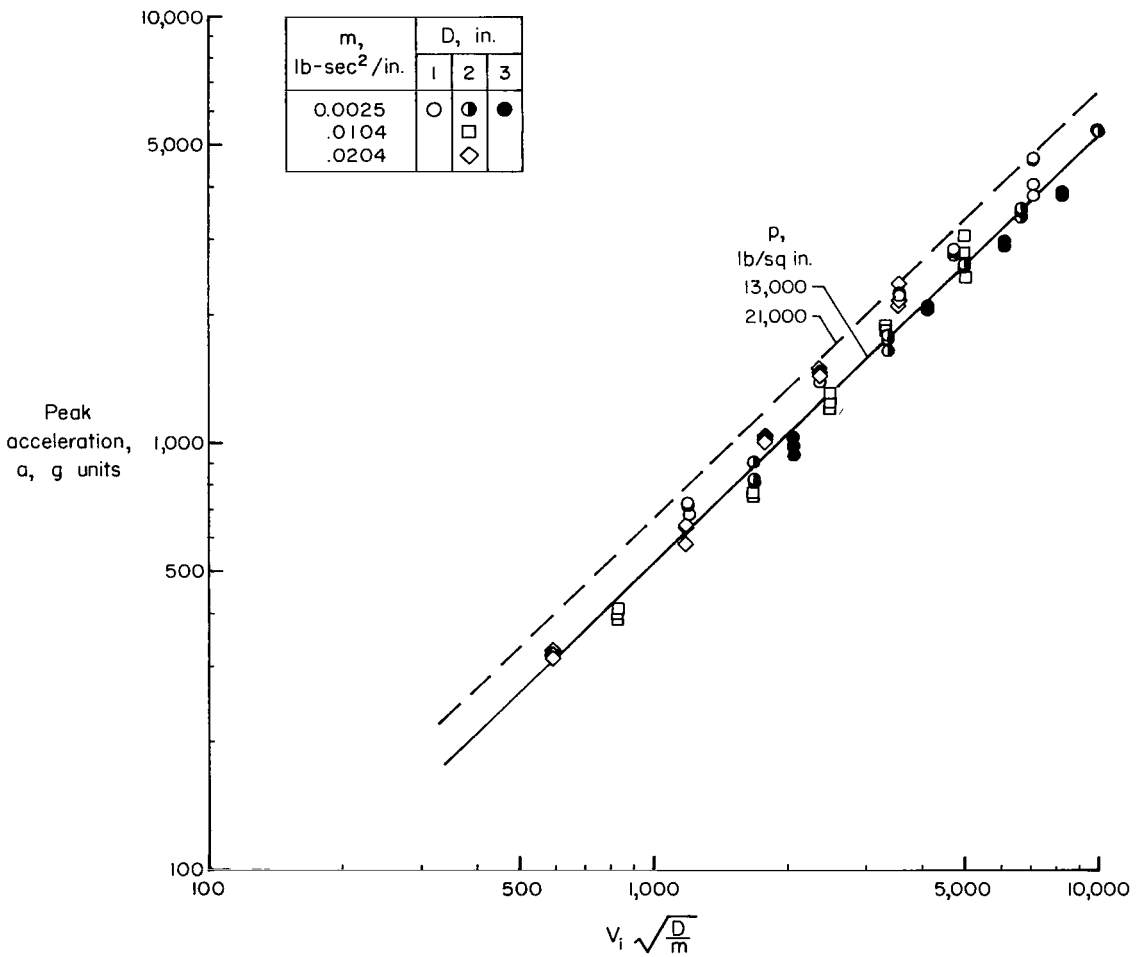

Figure 11.- Experimental and theoretical peak accelerations for impact of projectiles on lead targets. $a = V_i\sqrt{\frac{\pi D p}{m}}$.

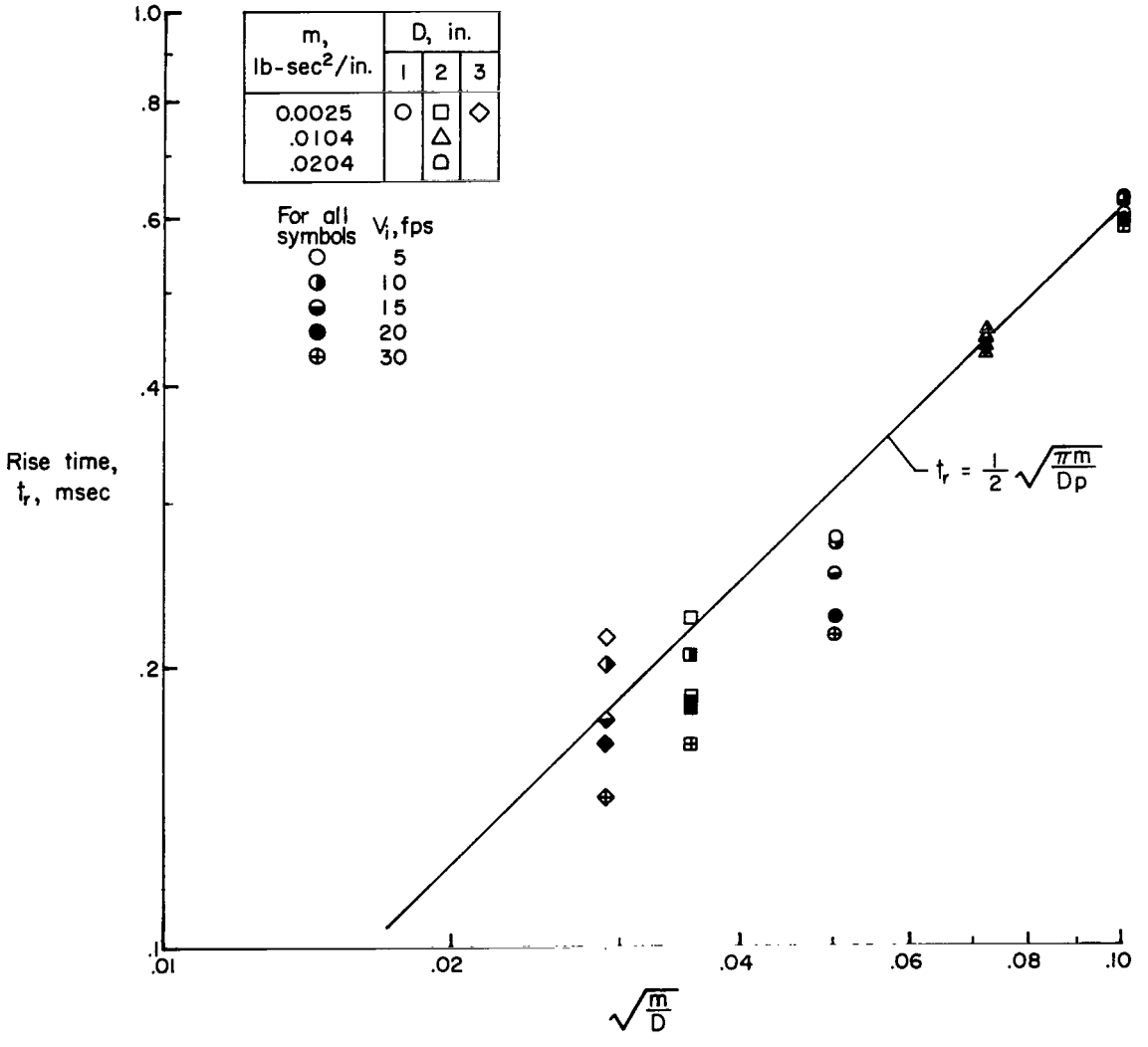

Figure 12.- Experimental and theoretical rise times for impact of projectiles on lead targets. p = 21,000 lb/sq in.

L-1670

L-1670

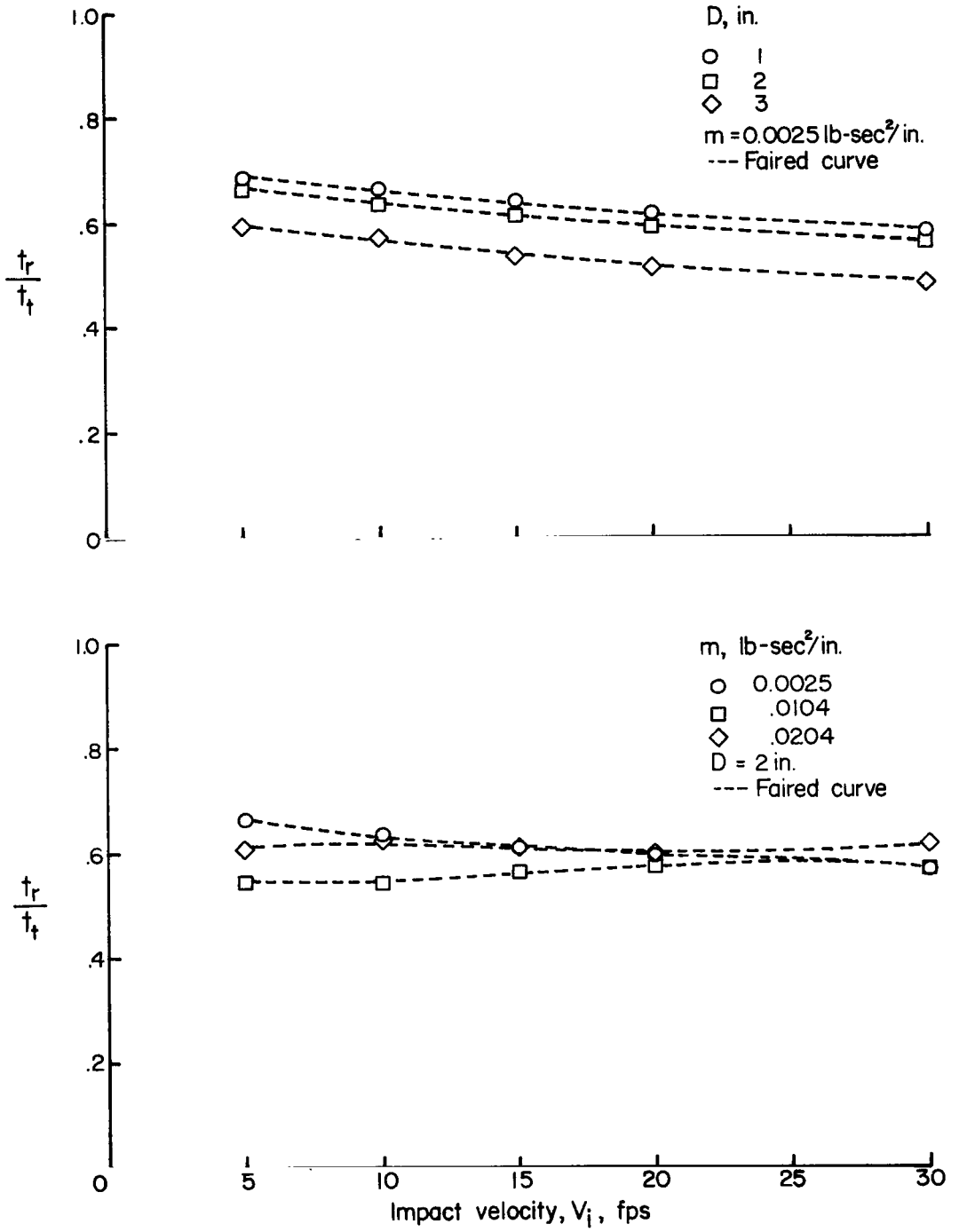

Figure 13.- Effect of projectile diameter and mass on characteristic times for impacts on lead targets.

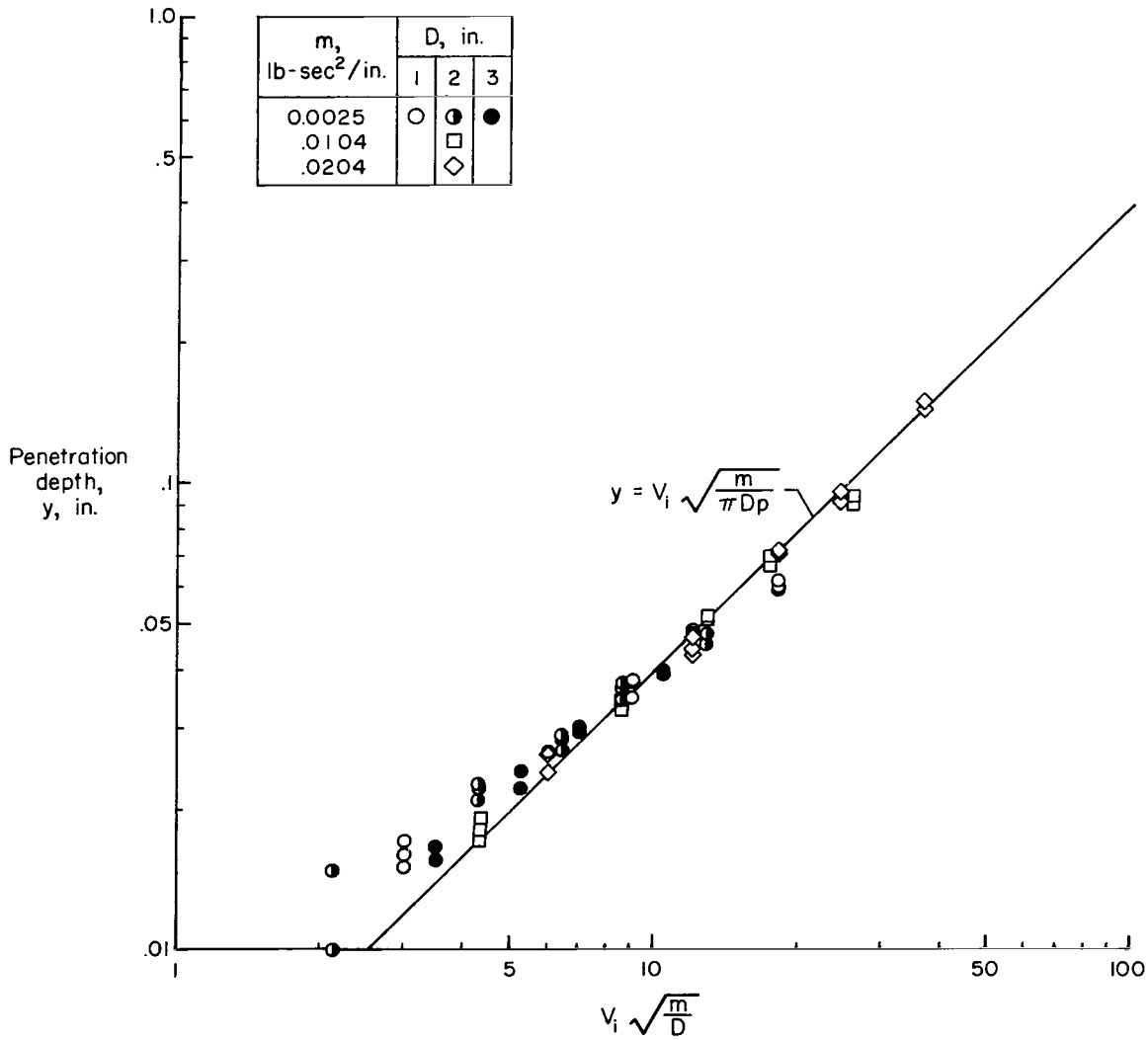

Figure 14.- Experimental and theoretical penetration depths resulting from the impact of projectiles on lead targets. p = 21,000 lb/sq in.

L-1670

L-1670

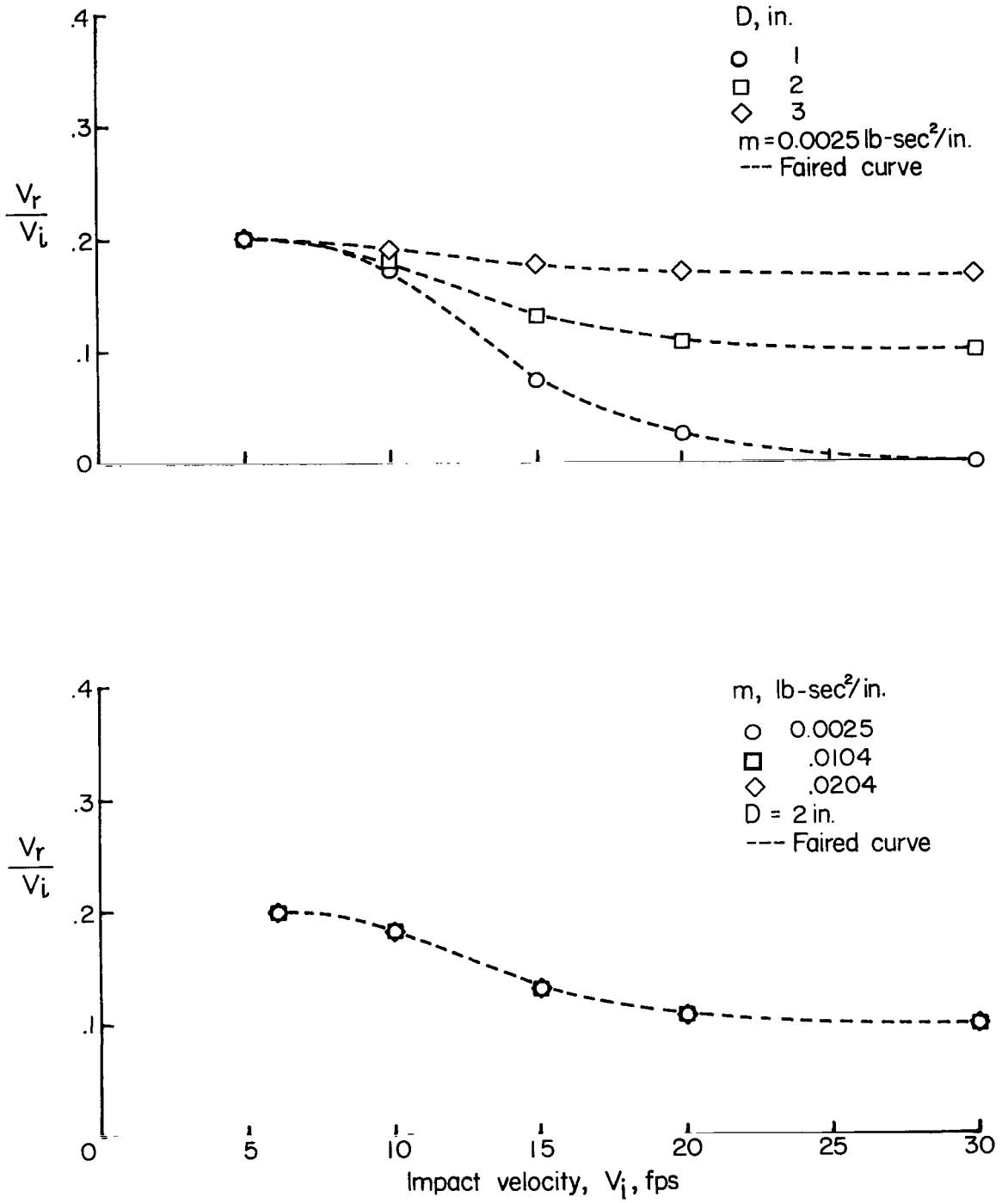

Figure 15.- Effect of projectile diameter and mass on restitution velocity measured during impact on balsa targets.

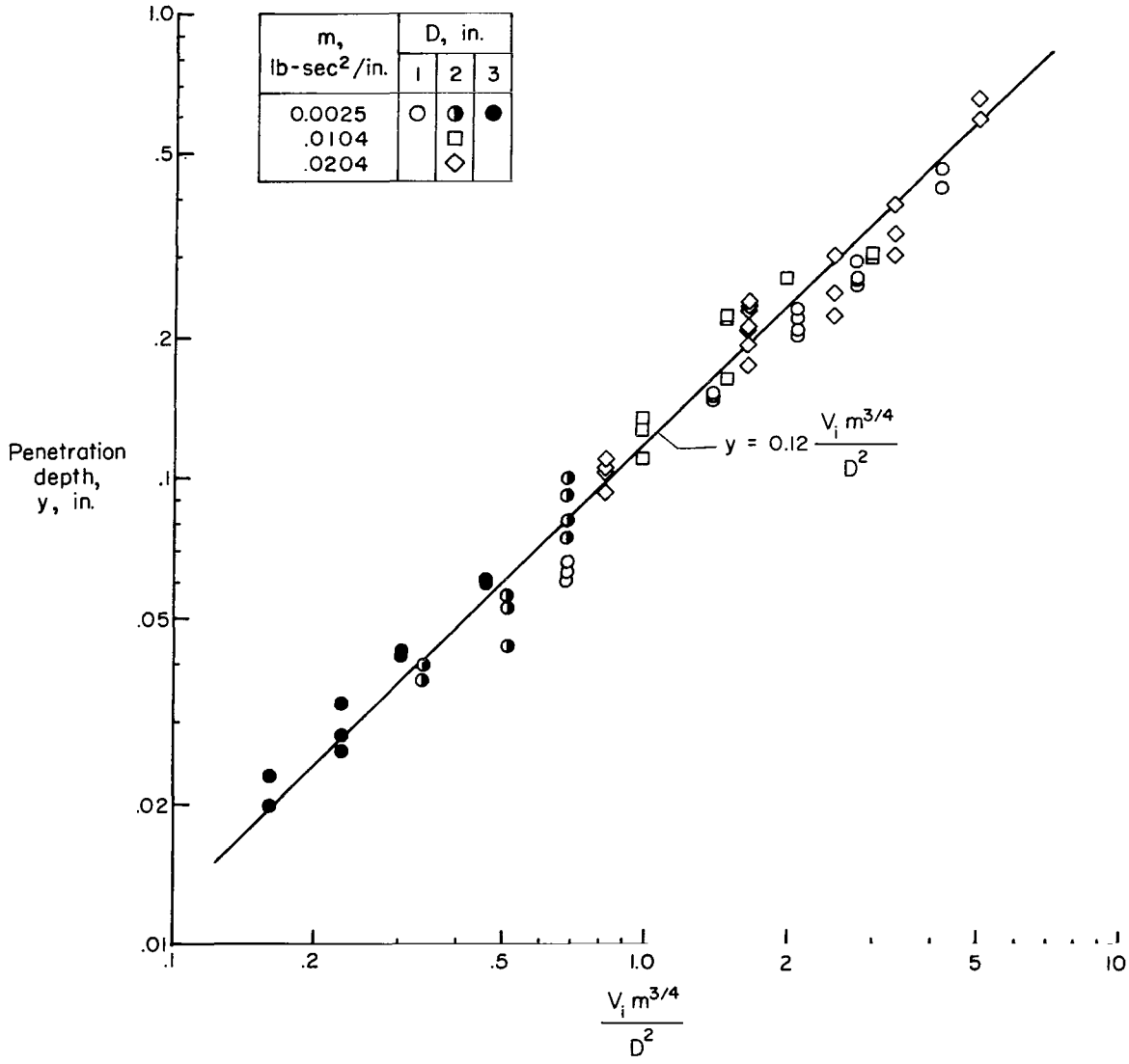

Figure 16.- Penetration depths measured during impact of projectiles on balsa targets.

L-1670

L-1670

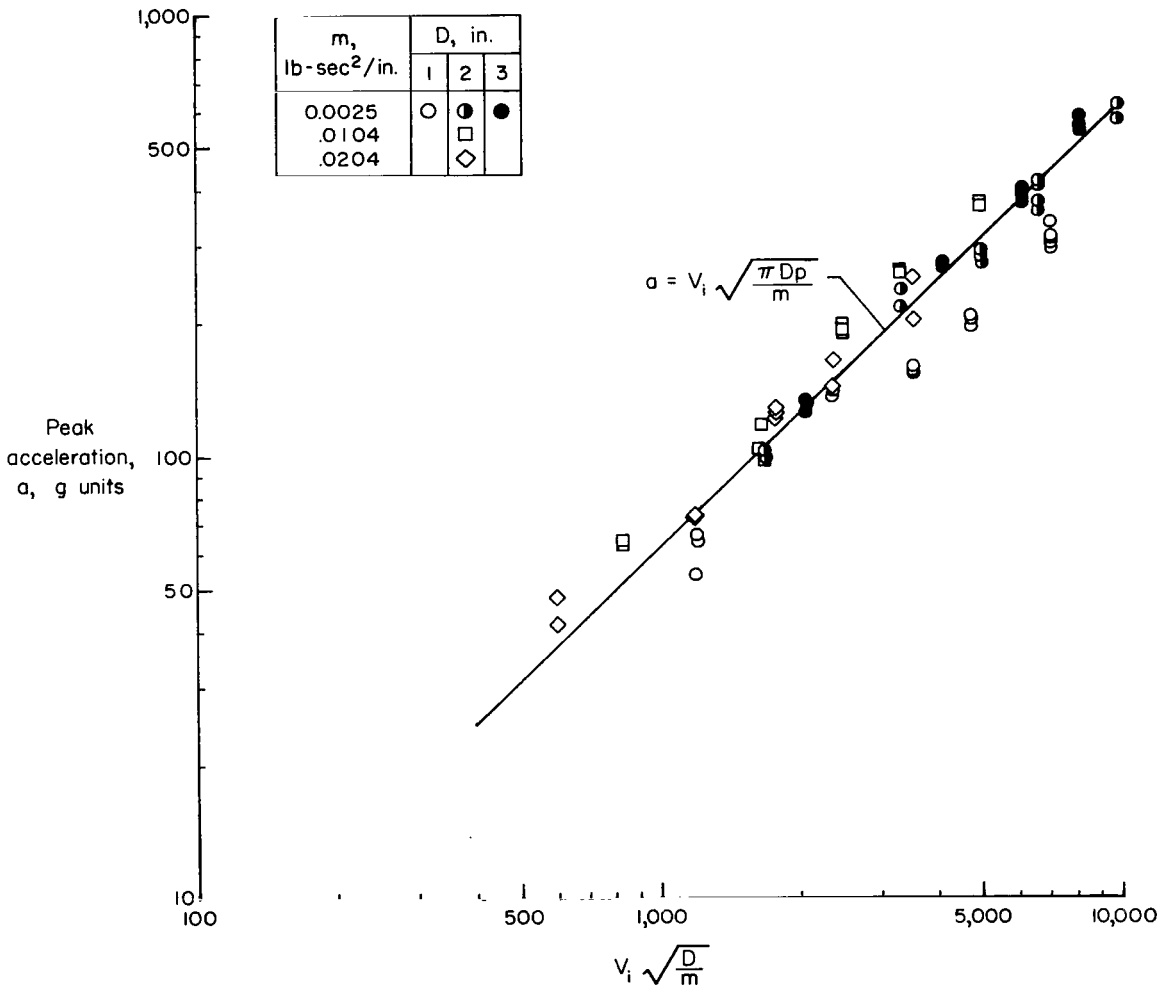

Figure 17.- Experimental and theoretical peak accelerations for impact of projectiles on balsa targets. p = 180 lb/sq in.

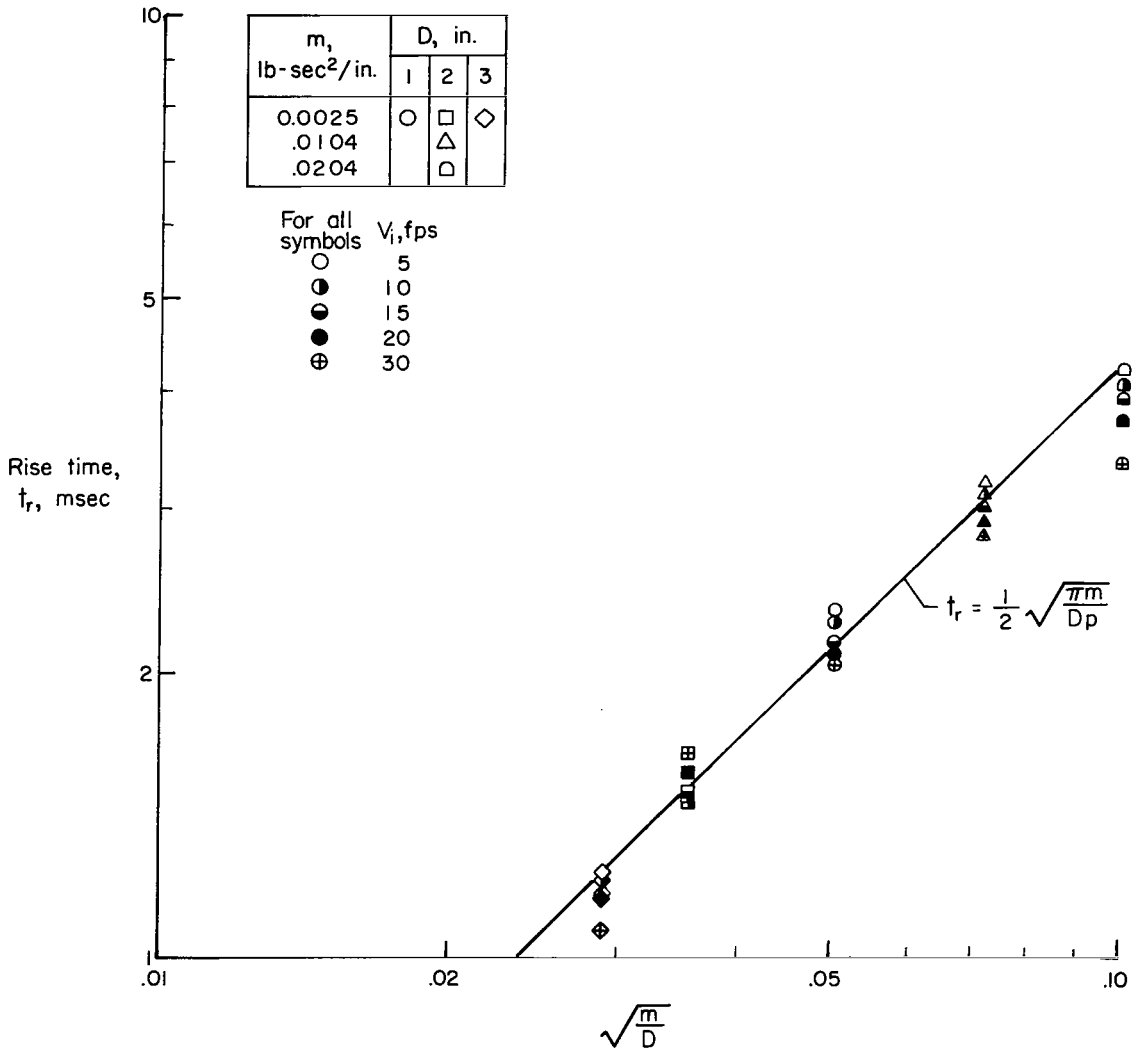

Figure 18.- Experimental and theoretical rise times for impact of projectiles on balsa targets. p = 435 lb/sq in.

L-1670

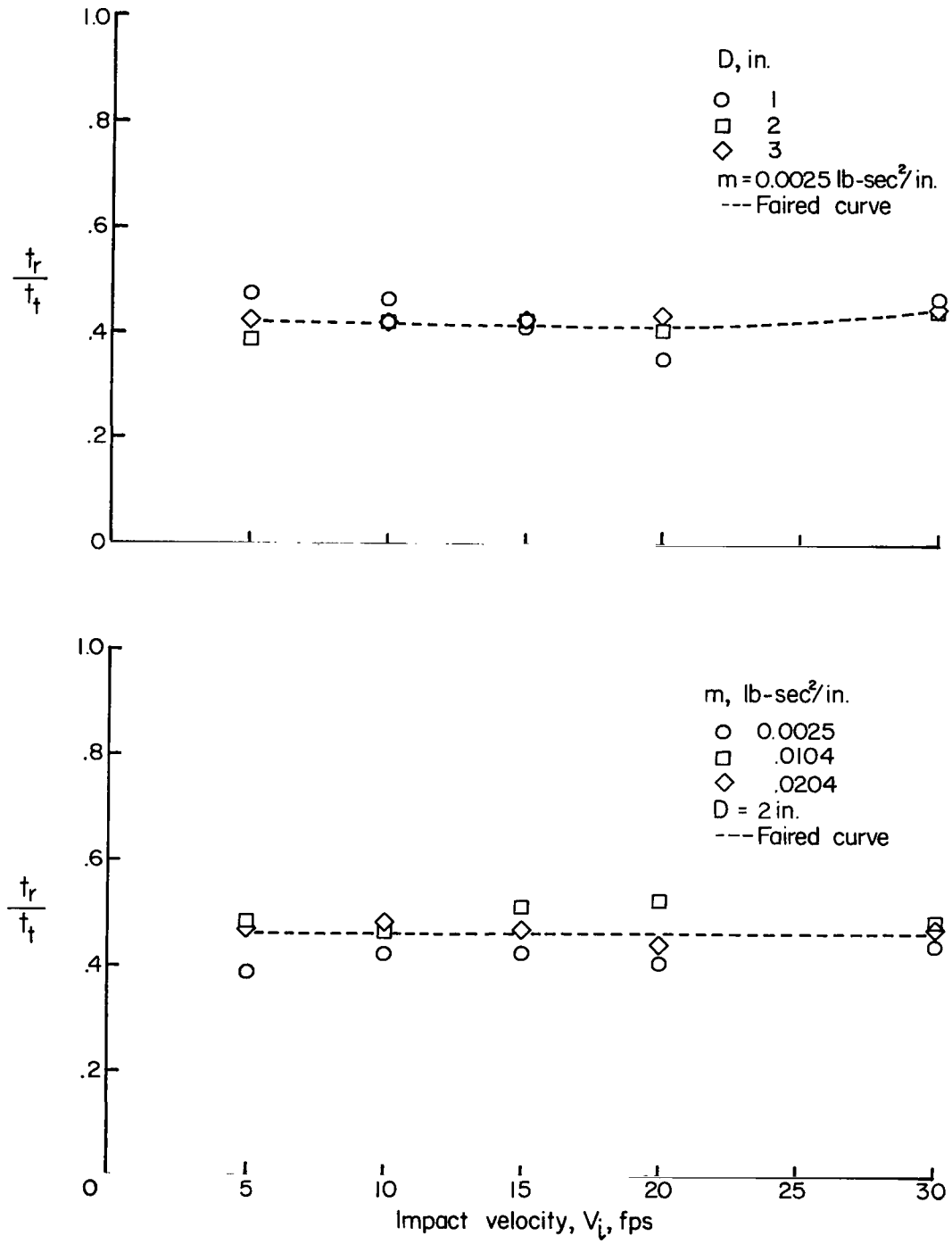

Figure 19.- Effect of projectile diameter and mass on characteristic times of impacts on balsa targets.

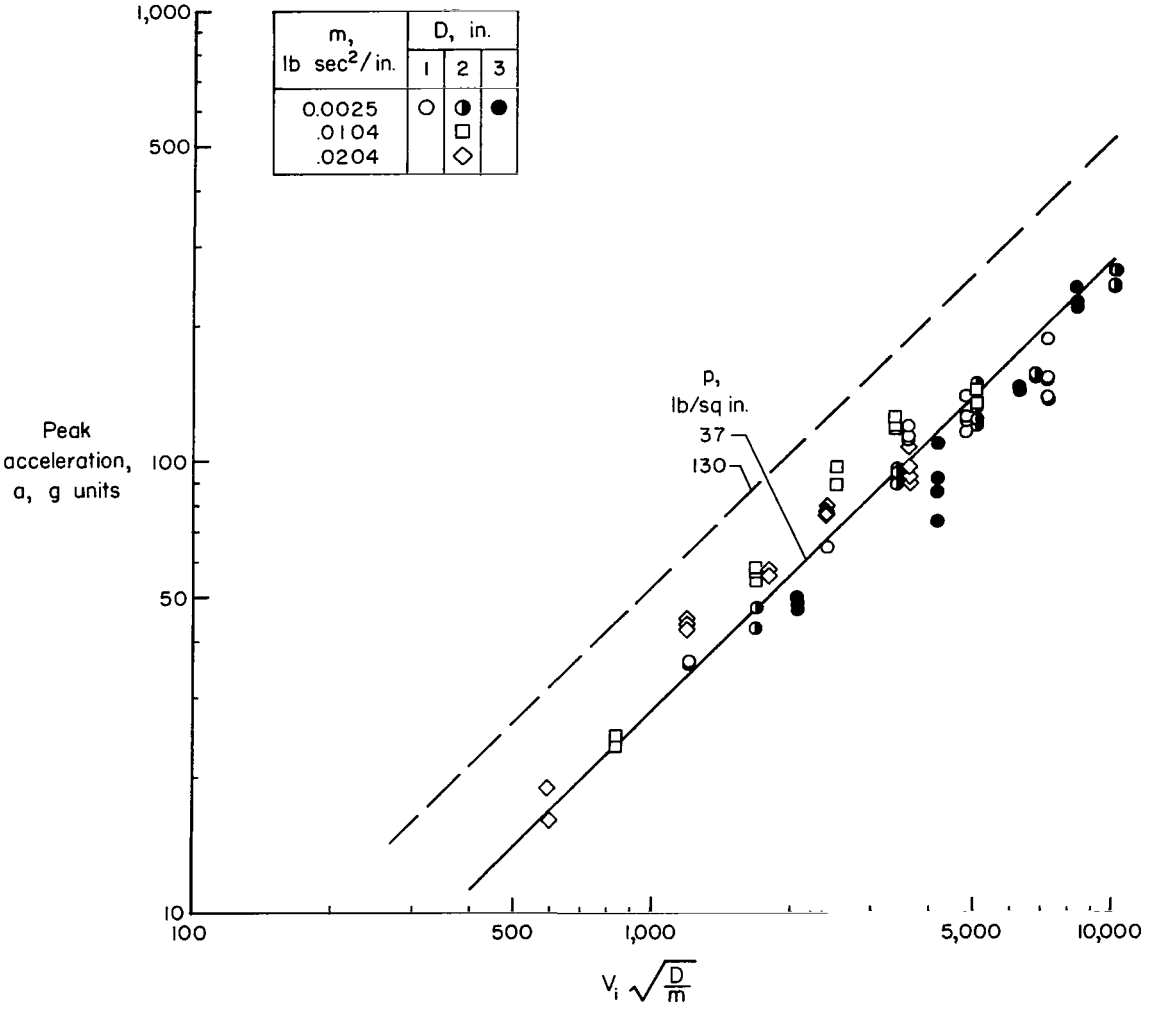

Figure 20.- Experimental and theoretical peak accelerations for impact of projectiles on sod targets. $a = V_i\sqrt{\frac{\pi Dp}{m}}$.

L-1670

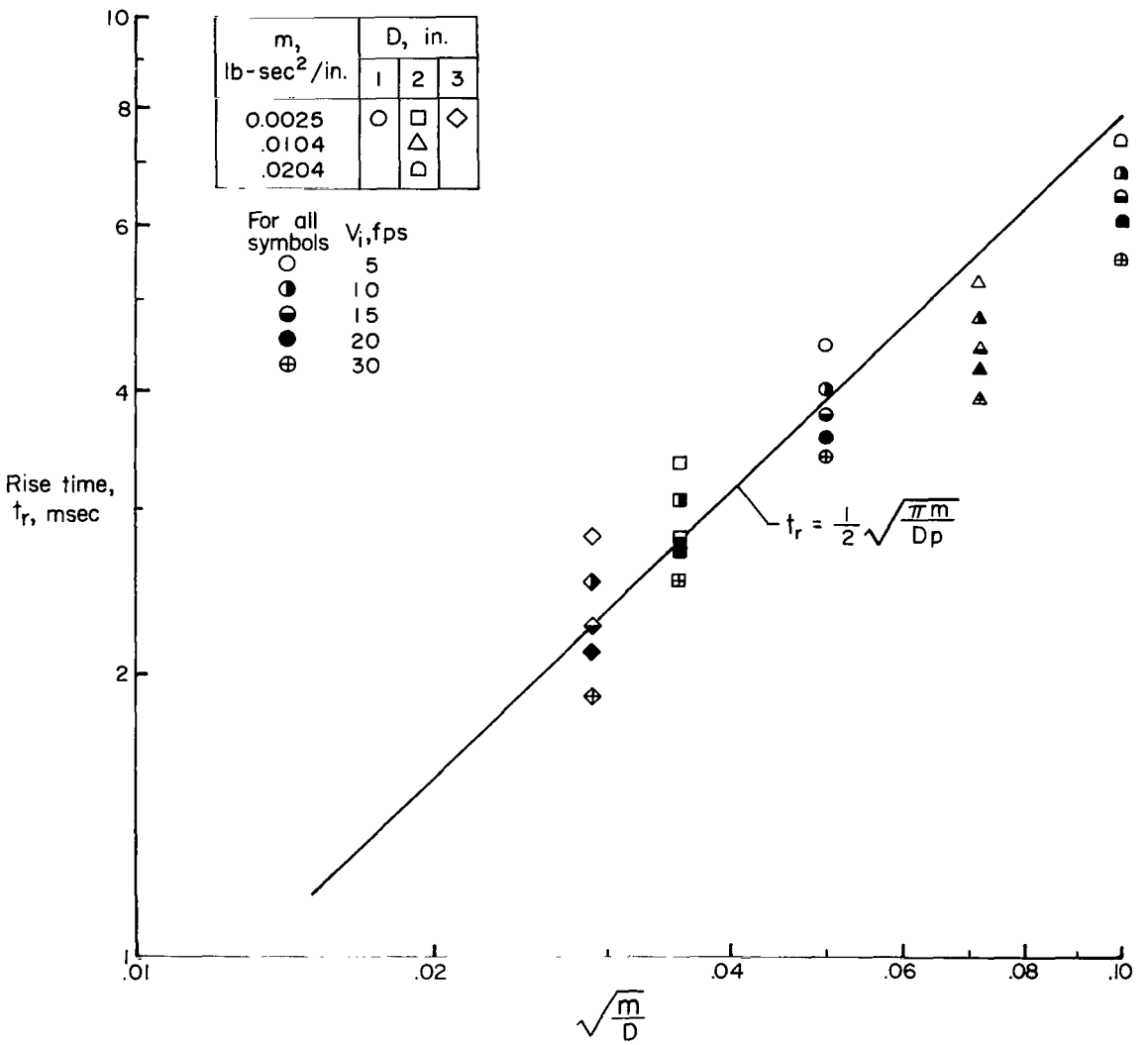

Figure 21.- Experimental and theoretical rise times for impact of projectiles on sod targets. p = 130 lb/sq in.

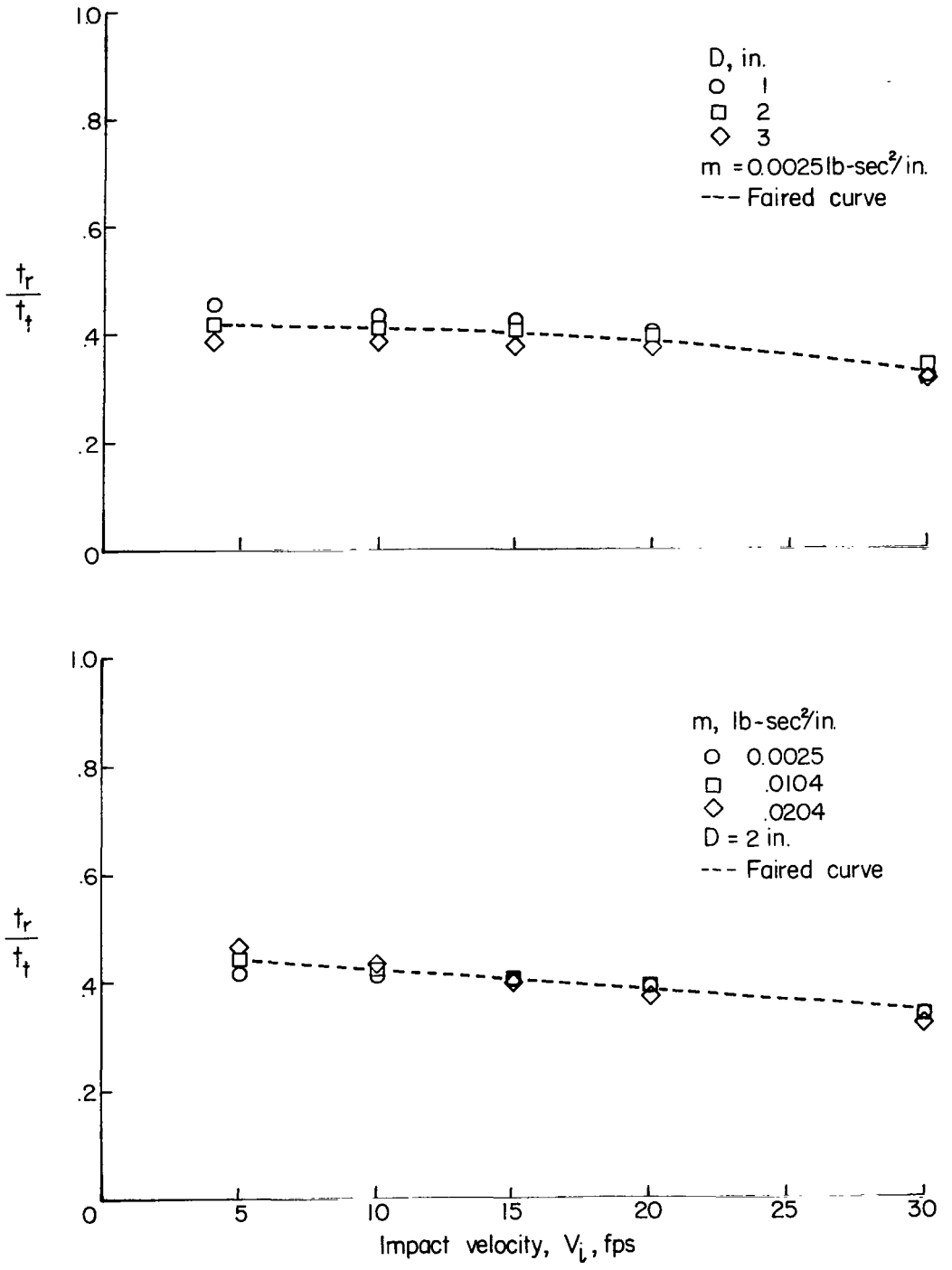

Figure 22.- Effect of projectile diameter and mass on characteristic times of impacts on sod targets.

L-1670

L-1670

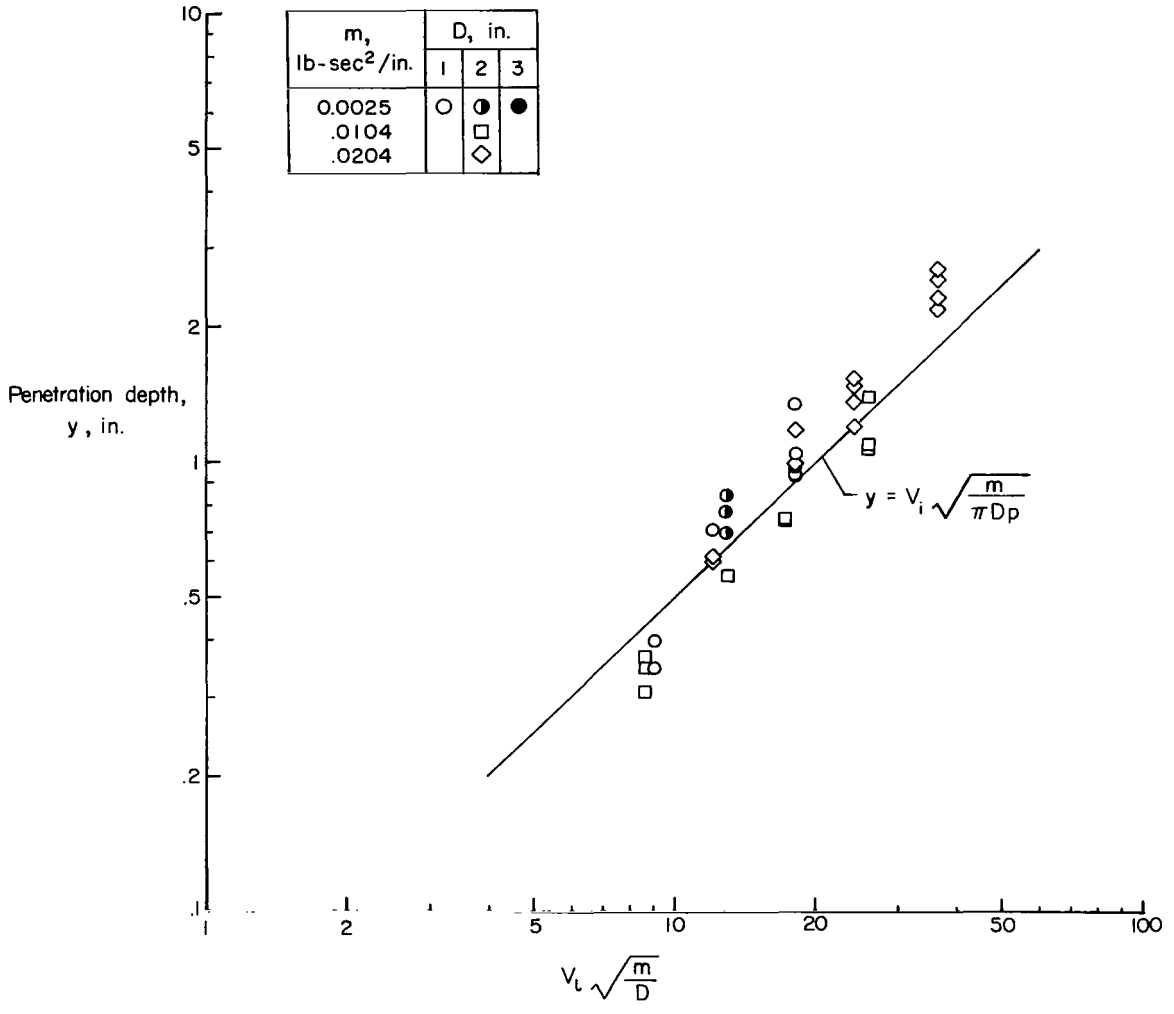

Figure 23.- Experimental and theoretical penetration depths resulting from the impact of projectiles on sod targets. p = 130 lb/sq in.

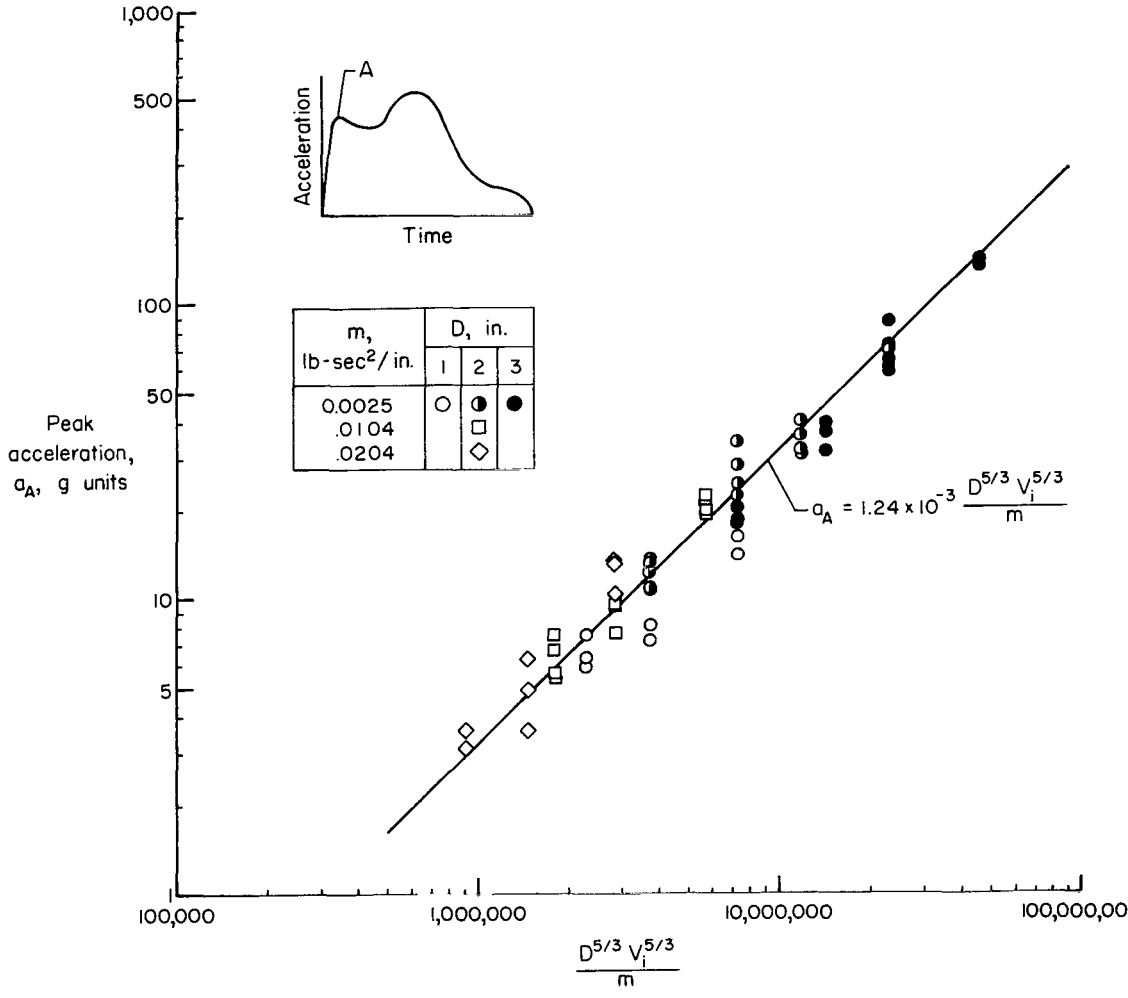

(a) Initial peak accelerations.

Figure 24.- Peak accelerations measured during the impact of projectiles on sand targets.

L-1670

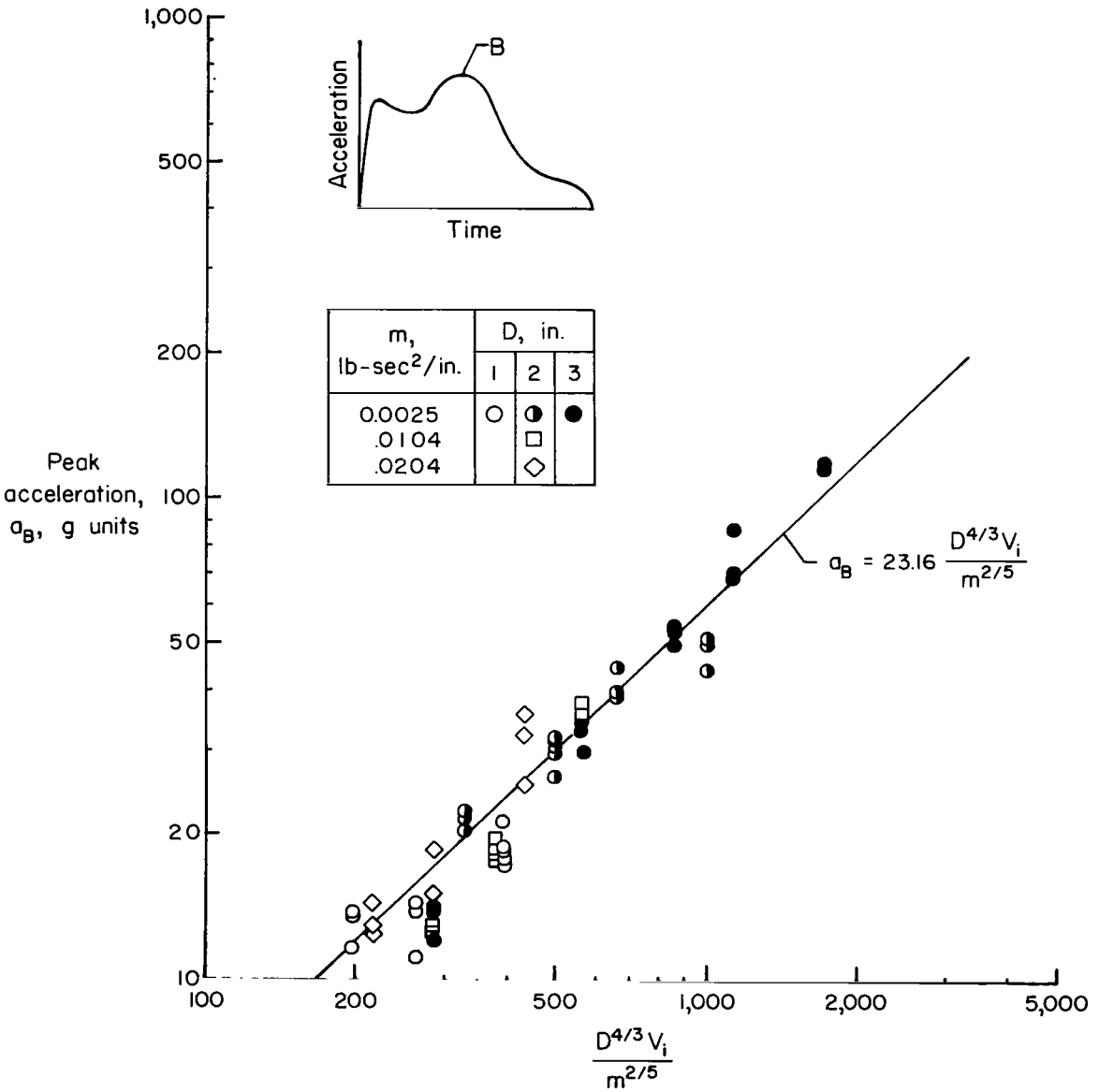

(b) Second peak accelerations.

Figure 24.- Concluded.

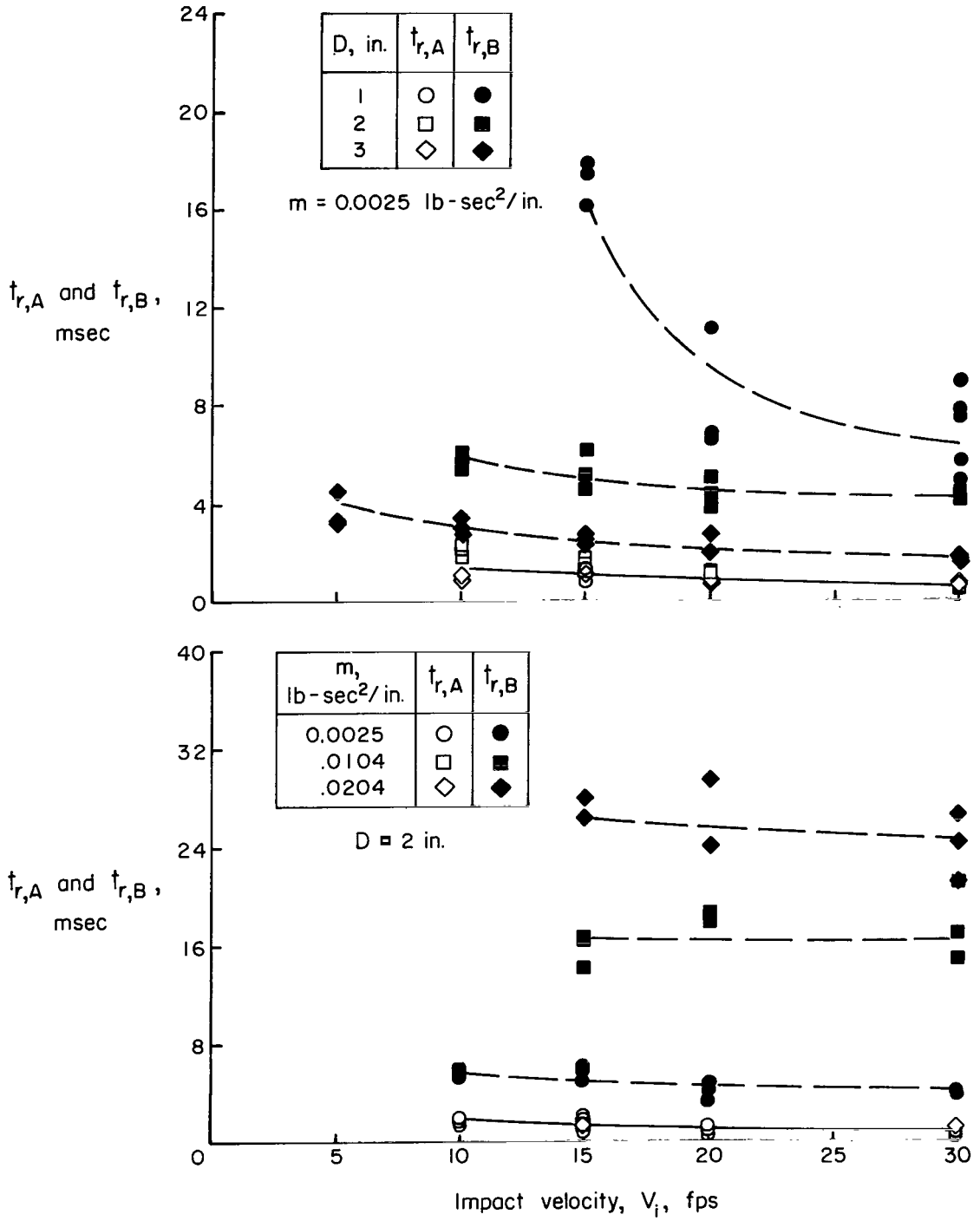

Figure 25.- Effect of projectile diameter and mass on rise times measured during impact on sand targets.

L-1670

L-1670

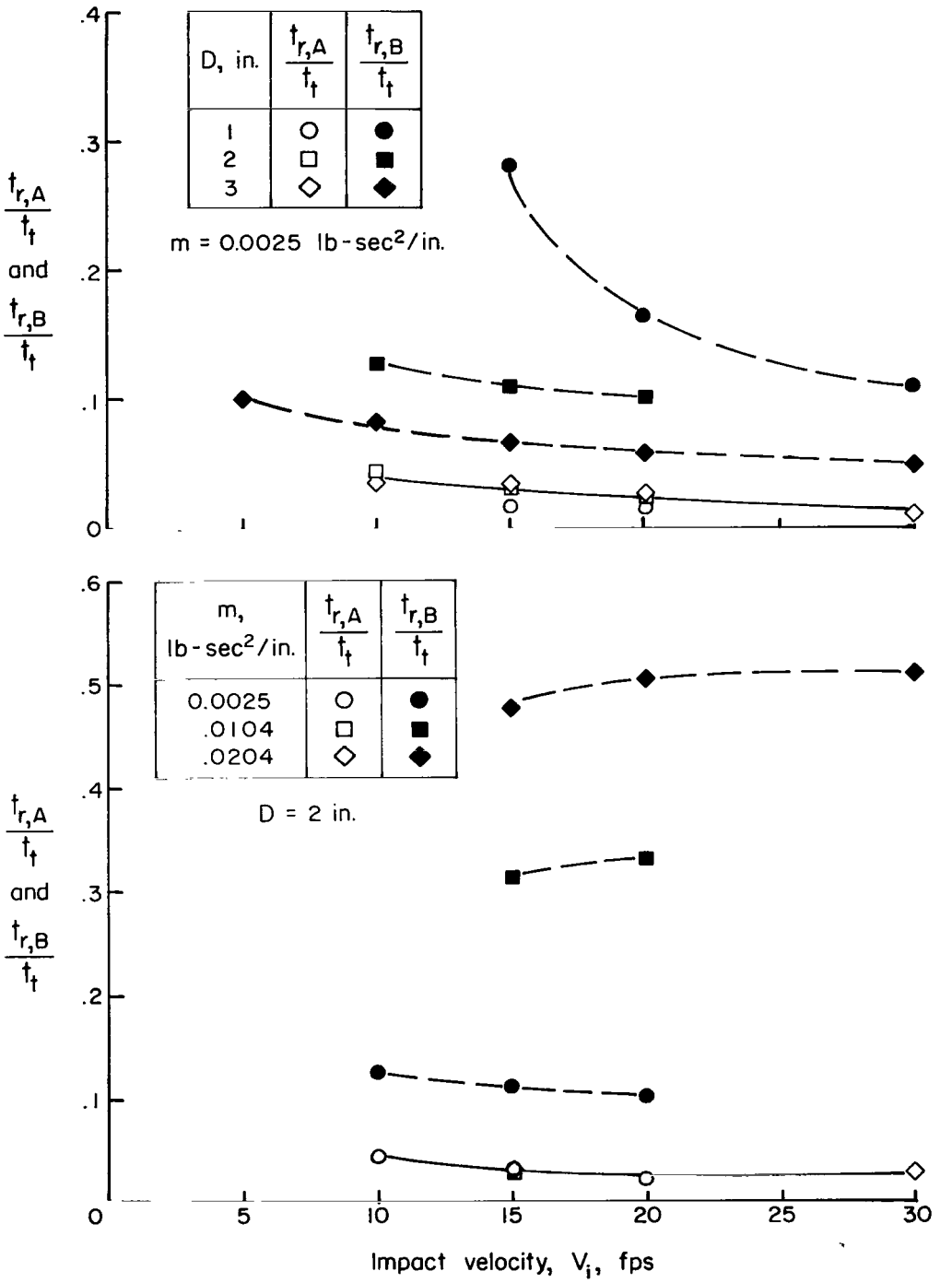

Figure 26.- Effect of projectile diameter and mass on characteristic times of impacts on sand targets.

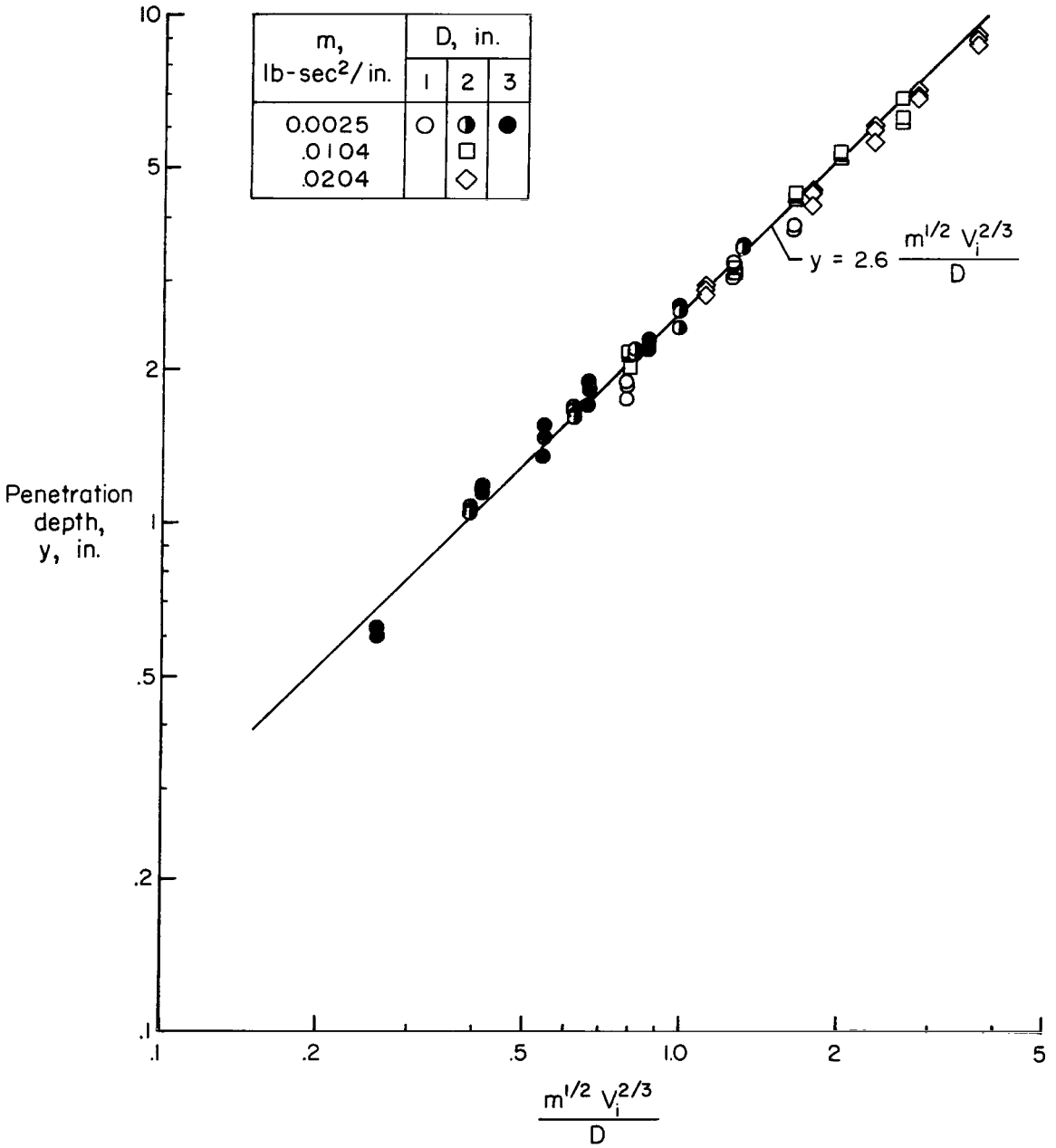

Figure 27.- Penetration depths resulting from the impact of projectiles on sand targets.

L-1670

L-1670

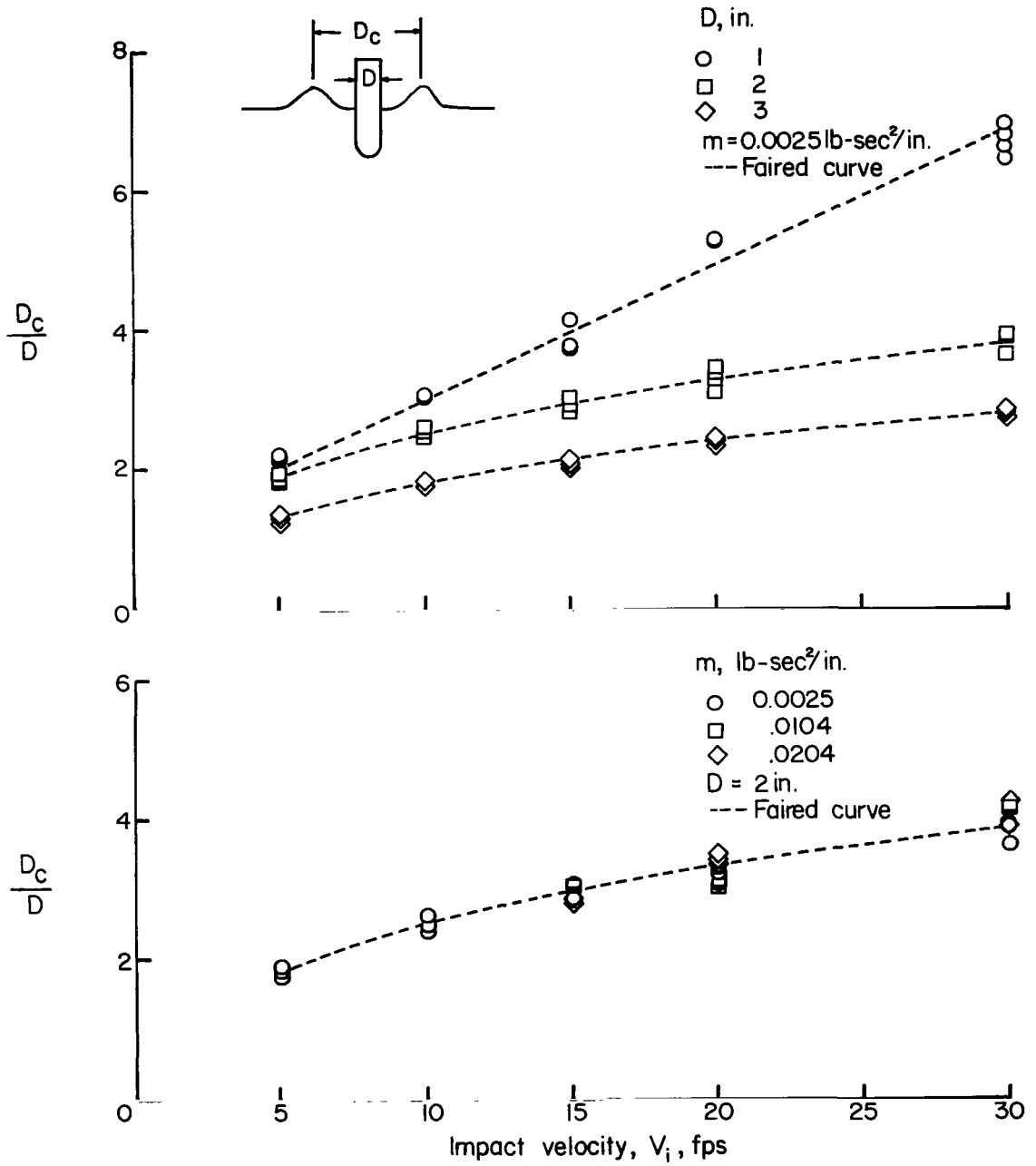

Figure 28.- Effect of projectile diameter and mass on blast-crater diameter resulting from impact on sand targets.

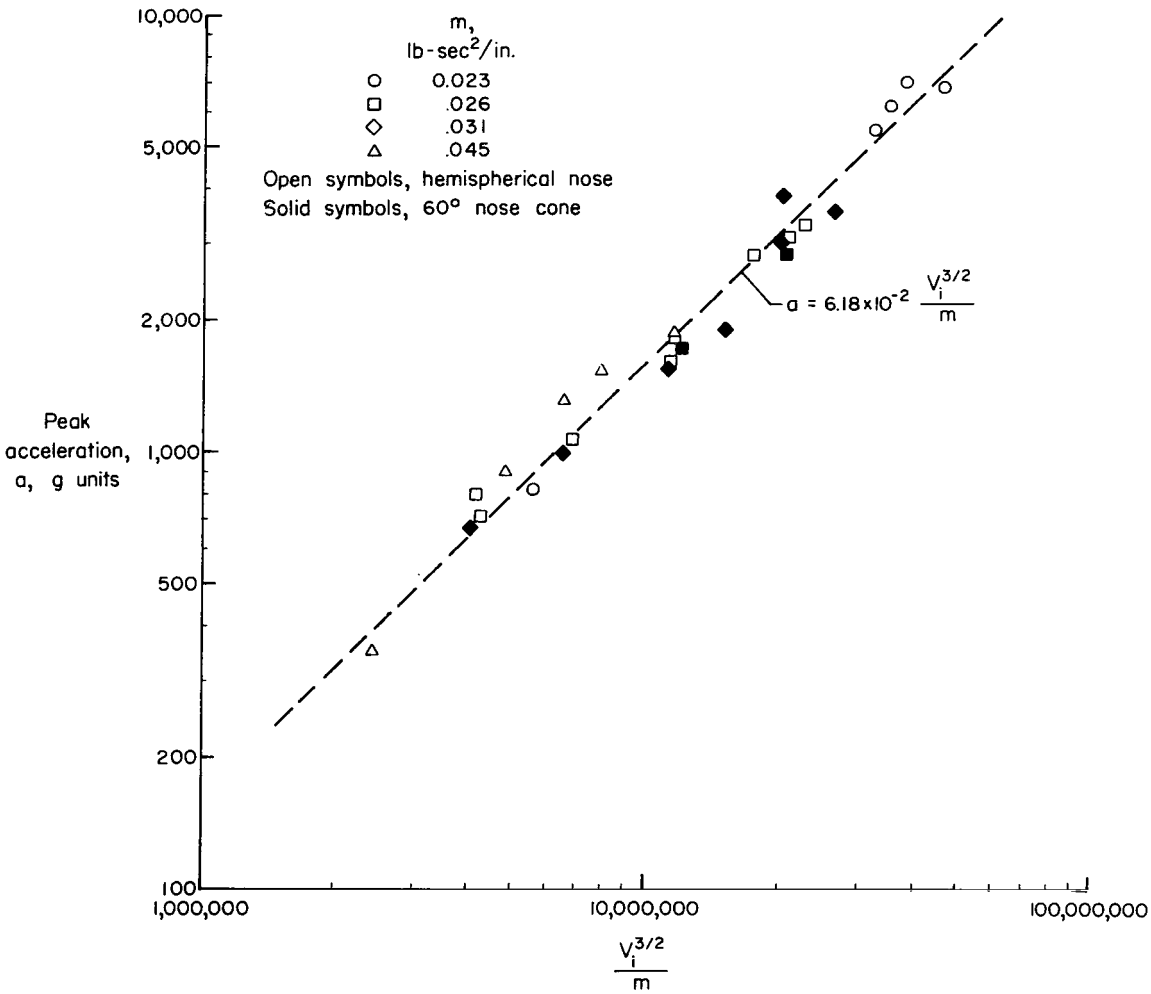

Figure 29.- Peak accelerations measured during high-velocity impacts of 3-inch-diameter projectiles in soil targets.

L-1670

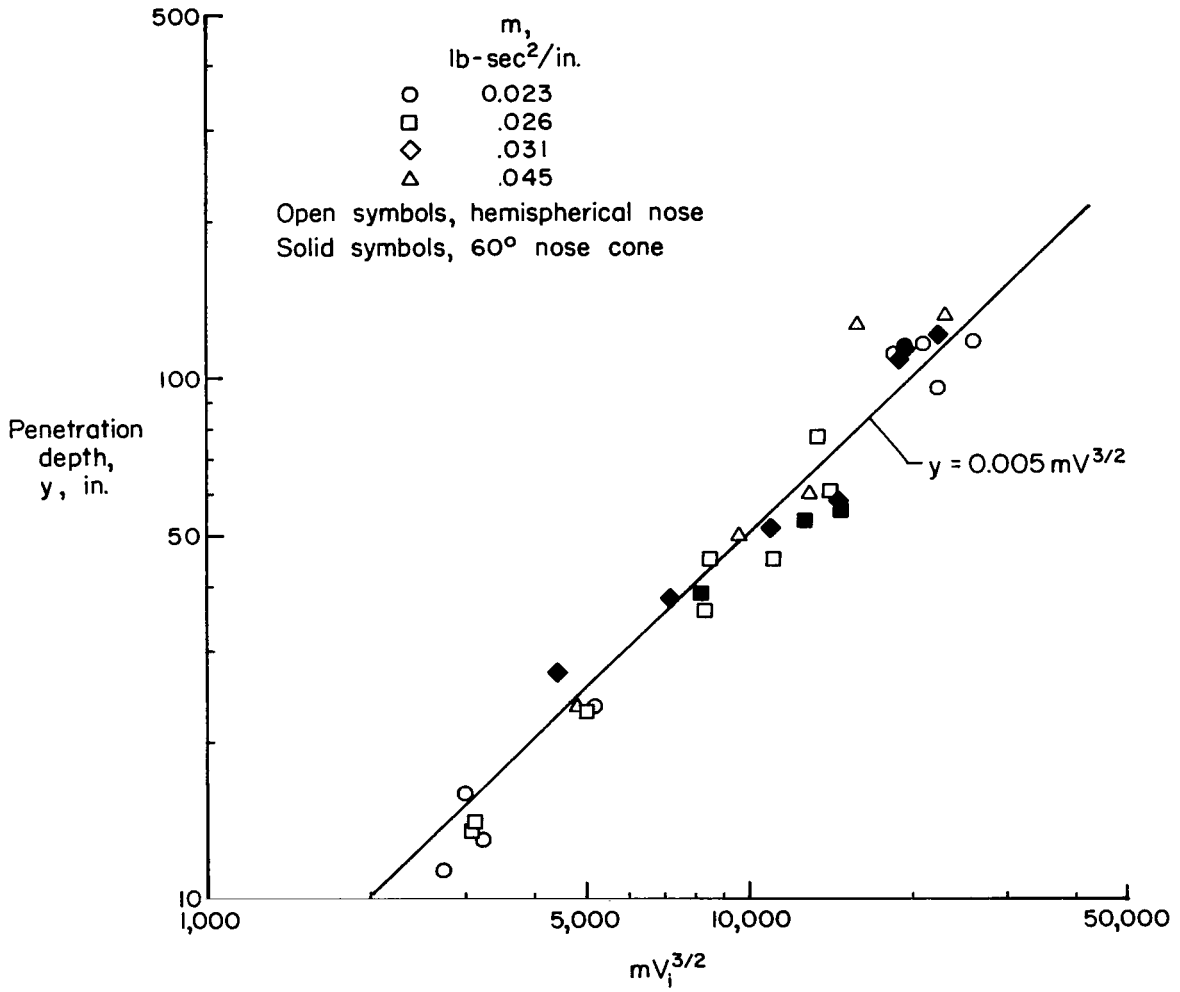

Figure 30.- Penetration depths resulting from high-velocity impacts of 3-inch-diameter projectiles in soil targets.

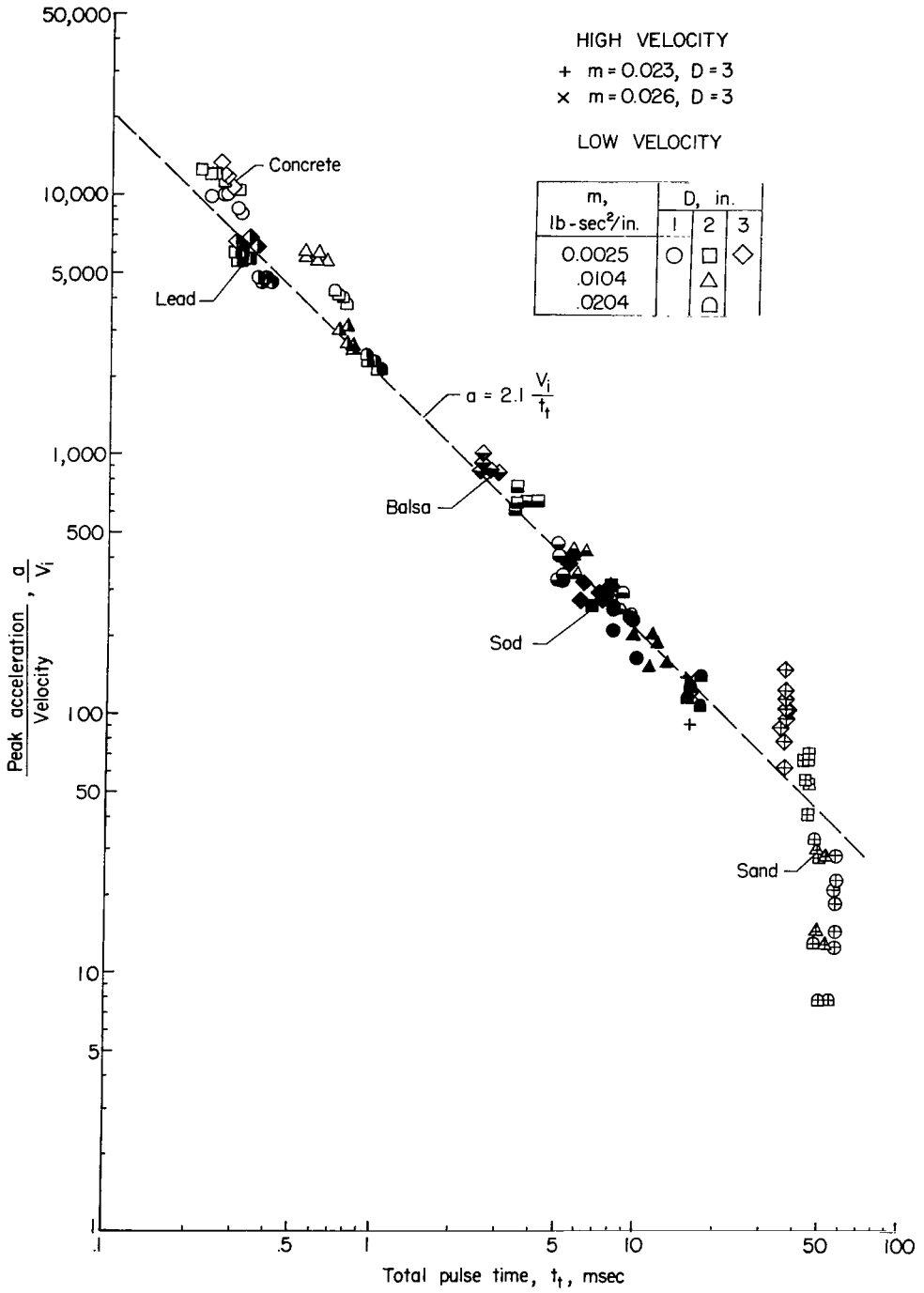

Figure 31.- Résumé of characteristics measured from acceleration time histories recorded during impact of projectiles on various target materials.

L-1670

L-1670

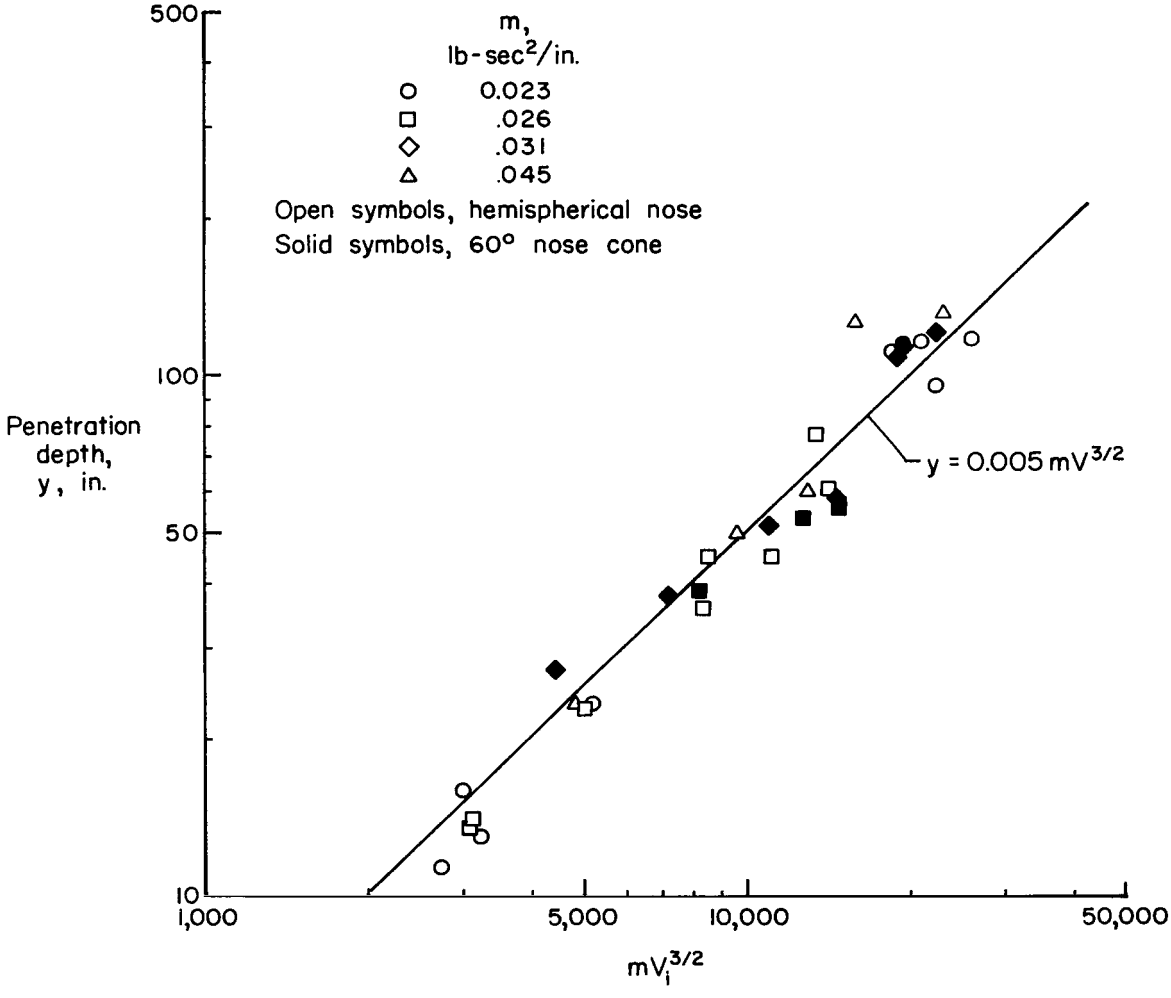

Figure 30.- Penetration depths resulting from high-velocity impacts of 3-inch-diameter projectiles in soil targets.

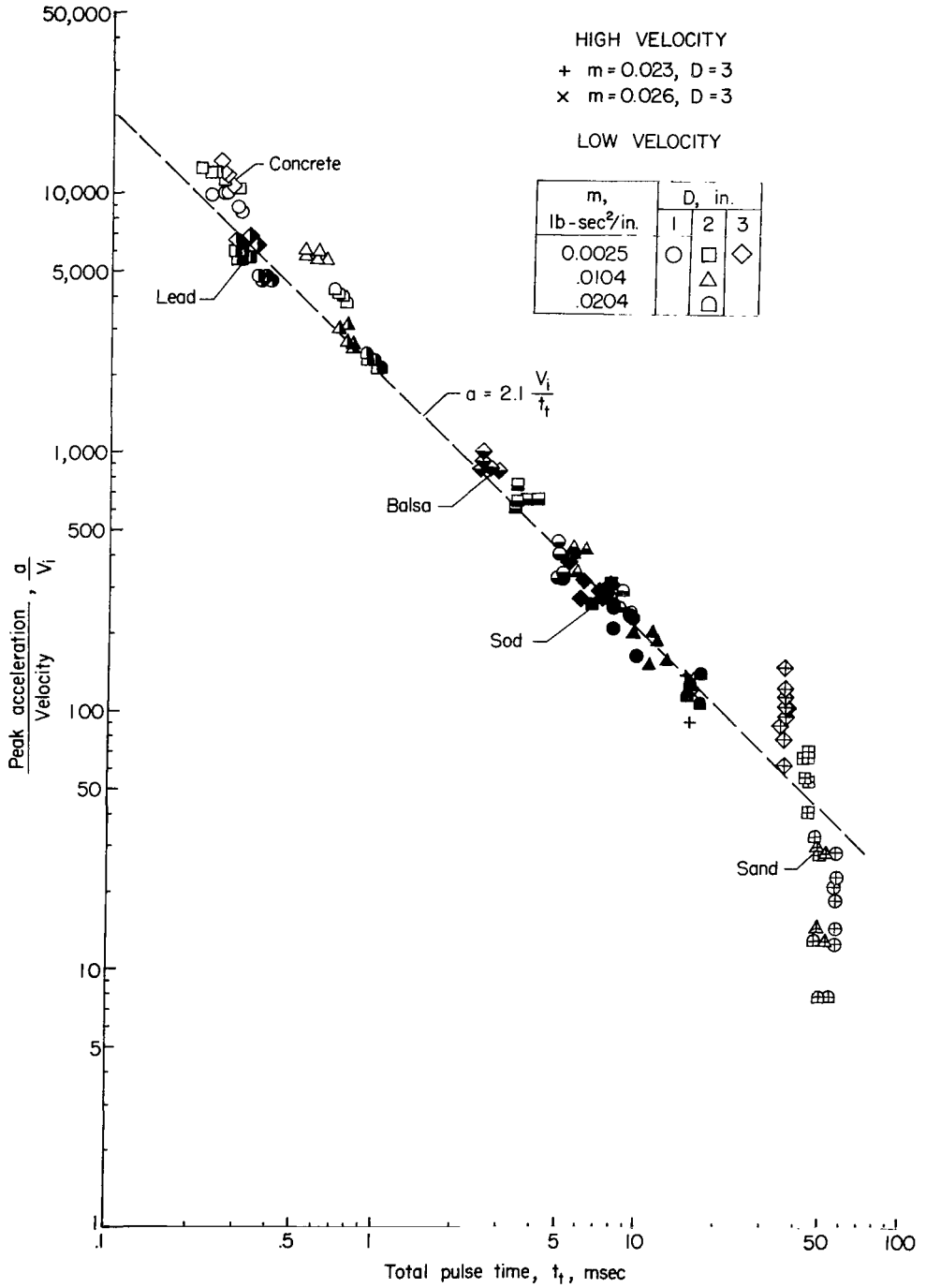

Figure 31.- Résumé of characteristics measured from acceleration time histories recorded during impact of projectiles on various target materials.

L-1670

L-1670

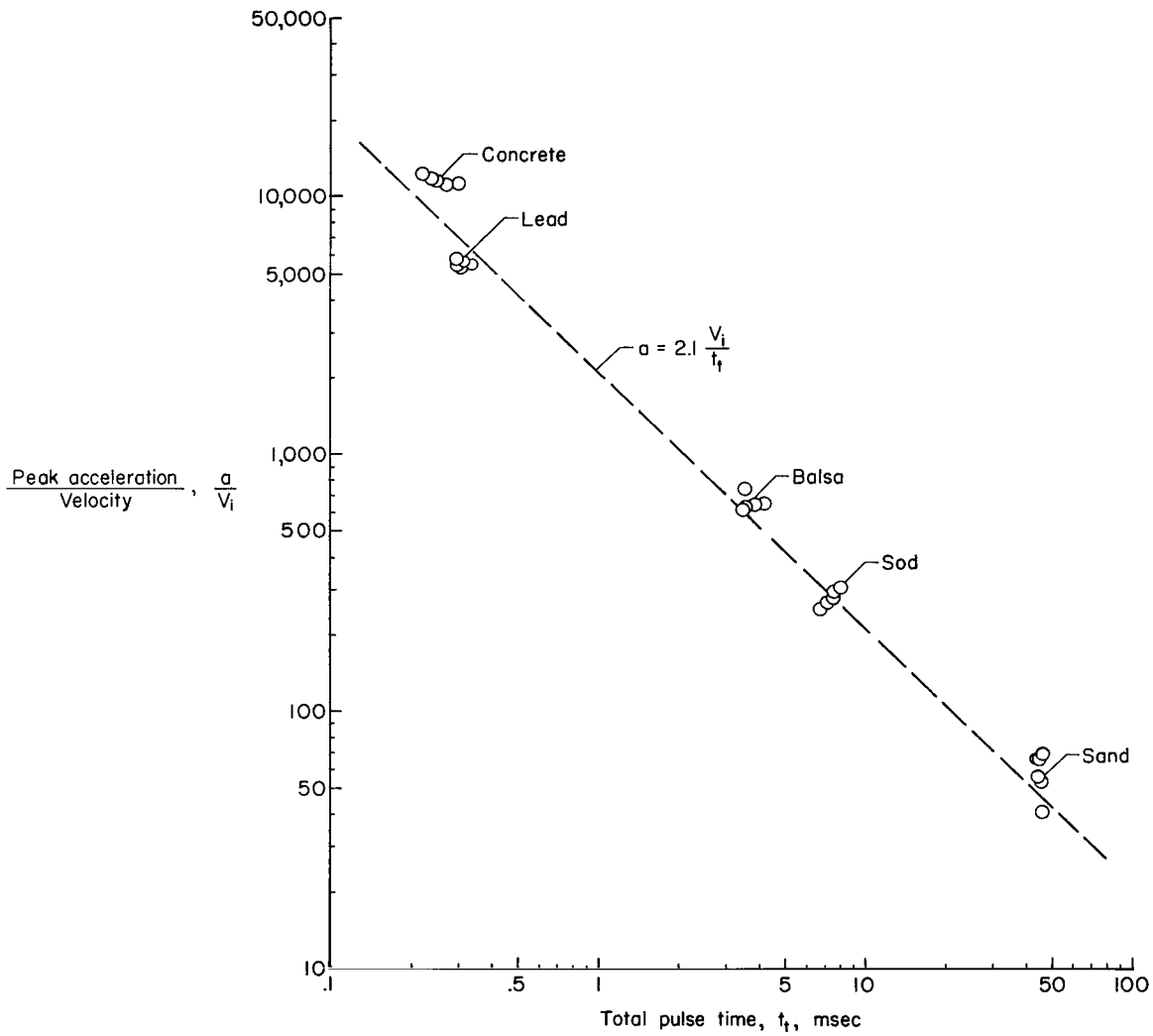

Figure 32.- Résumé of characteristics measured from acceleration time histories recorded during impact of a projectile on various target materials. m = 0.0025 lb-sec^2/in.; D = 2 in.

NASA-Langley, 1962 L-1670